

Resonantly enhanced and diminished strong-field gravitational-wave fluxes

Éanna E. Flanagan,¹ Scott A. Hughes,^{2,3,4} and Uchupol Ruangsri²

¹*Center for Radiophysics and Space Research, Cornell University, Ithaca, NY 14853, USA*

²*Department of Physics and MIT Kavli Institute, MIT, Cambridge, MA 02139, USA*

³*Canadian Institute for Theoretical Astrophysics, University of Toronto,*

60 St. George St., Toronto, ON M5S 3H8, Canada

⁴*Perimeter Institute for Theoretical Physics, Waterloo, ON N2L 2Y5, Canada*

(Dated: August 21, 2012)

The inspiral of a stellar mass ($1 - 100 M_\odot$) compact body into a massive ($10^5 - 10^7 M_\odot$) black hole has been a focus of much effort, both for the promise of such systems as astrophysical sources of gravitational waves, and because they are a clean limit of the general relativistic two-body problem. Our understanding of this problem has advanced significantly in recent years, with much progress in modeling the “self force” arising from the small body’s interaction with its own spacetime deformation. Recent work has shown that this self interaction is especially interesting when the frequencies associated with the orbit’s θ and r motions are in an integer ratio: $\Omega_\theta/\Omega_r = \beta_\theta/\beta_r$, with β_θ and β_r both integers. In this paper, we show that key aspects of the self interaction for such “resonant” orbits can be understood with a relatively simple Teukolsky-equation-based calculation of gravitational-wave fluxes. We show that fluxes from resonant orbits depend on the relative phase of radial and angular motions. The purpose of this paper is to illustrate in simple terms how this phase dependence arises using tools that are good for strong-field orbits, and to present a first study of how strongly the fluxes vary as a function of this phase and other orbital parameters. Future work will use the full dissipative self force to examine resonant and near resonant strong-field effects in greater depth.

PACS numbers: 04.30.-w, 04.25.Nx, 04.70.-s

I. INTRODUCTION

Our understanding of the two-body problem in general relativity has advanced substantially in the past decade. Besides the celebrated breakthroughs in numerical relativity [1–3] which have opened the field of binary phenomenology in general relativity, there has been great progress in understanding the extreme mass ratio limit of this problem, when one member of the binary is much smaller than the other. This limit is of great interest in describing astrophysical extreme mass ratio binaries (a particularly interesting source for space-based gravitational-wave measurements) [4], and as a limiting form of the more generic two-body problem [5, 6].

Most efforts to model extreme mass ratio binaries have focused on the computation of *self forces* (see Ref. [7] for a recent comprehensive review). Consider a small body orbiting a black hole. At zeroth order in the small body’s mass, its motion is described as a geodesic of the black hole spacetime. At first order in this mass, the black hole’s spacetime is slightly deformed. This deformation changes the trajectory that the small body follows, pushing it away from the background spacetime’s geodesic. It is useful to regard the change to the trajectory as arising from a self force which modifies the geodesic equations typically used to describe black hole orbits. Conceptually, it is useful to split the self force into two pieces: A time-symmetric *conservative* piece, and a time-asymmetric *dissipative* piece. On average, the impact of the conservative contribution is to shift orbital frequencies away from their geodesic values. The

dissipative self force is equivalent, on average, to a slow evolution of the otherwise conserved constants (e.g., the orbital energy and angular momentum) which characterize geodesic orbits. It makes the largest contribution to an orbit’s phase evolution. The conservative piece makes a smaller (though still significant) contribution which accumulates secularly over many orbits [8].

Recent work by Flanagan and Hinderer [9] (hereafter FH) using a post-Newtonian (pN) approximation to the self force together with fully relativistic orbital dynamics has shown that a small body’s self interaction becomes particularly important near *resonances*. The background geodesic motion can be characterized by three orbital frequencies with respect to Boyer-Lindquist time: A radial frequency Ω_r , a polar frequency Ω_θ , and an axial frequency Ω_ϕ . In the weak-field (large separation) limit, these three frequencies asymptote to the Newtonian Kepler frequency. In the strong-field, these frequencies can differ significantly, with $\Omega_r < \Omega_\theta < \Omega_\phi$. Resonant orbits are ones for which the radial and angular motions become commensurate: $\Omega_\theta/\Omega_r = \beta_\theta/\beta_r$, where β_θ and β_r are integers with no common factors. On such orbits, components of the self interaction which normally “average away” when examined over a full orbital period instead combine coherently, substantially changing their impact on the system’s evolution.

For the purpose of our background discussion, it is useful to include more details from FH’s analysis of how resonant effects arise. Consider a body of mass μ moving on a bound trajectory near a Kerr black hole of mass M , with $\mu \ll M$. FH note that one can describe the motion of this body using action-angle variables and correctly account-

ing for how the integrals which parameterize geodesic orbits evolve due to the self force. Writing the angle variables $q_\alpha = (q_t, q_r, q_\theta, q_\phi)$ (which describe motions in the t , r , θ , and ϕ directions of Boyer-Lindquist coordinates), and writing the integrals associated with geodesic motion $J_i = (E, L_z, Q)$ (with E the energy, L_z the axial angular momentum, and Q the Carter constant), the equations of motion describing the system are [10]

$$\frac{dq_\alpha}{d\tau} = \omega_\alpha(\mathbf{J}) + \epsilon g_\alpha^{(1)}(q_r, q_\theta, \mathbf{J}) + O(\epsilon^2), \quad (1.1)$$

$$\frac{dJ_i}{d\tau} = \epsilon G_i^{(1)}(q_r, q_\theta, \mathbf{J}) + O(\epsilon^2). \quad (1.2)$$

The time parameter τ is proper time along the orbit; the parameter $\epsilon = \mu/M$, the system's mass ratio. The $\omega_{r,\theta,\phi}$ are fundamental frequencies with respect to proper time associated with bound Kerr geodesic orbits. The forcing functions $g_\alpha^{(1)}$ and $G_i^{(1)}$ arise from the first-order self force. FH also include discussion of second-order forcing functions, which we do not need for this synopsis; see Ref. [9] for further discussion.

At order ϵ^0 , Eqs. (1.1) and (1.2) simply describe geodesics of Kerr black holes: The integrals of the motion are constant, and each angle variable evolves according to its associated frequency. The leading adiabatic dissipative correction to this motion can be found by dropping the forcing term $g_\alpha^{(1)}$ and replacing $G_i^{(1)}$ by $\langle G_i^{(1)} \rangle$, the average of this forcing term over the 2-torus parameterized by q_θ and q_r [10]. To compute this torus-averaged self force, it is sufficient to use the radiative approximation [8], which includes only the radiative contributions to the self interaction and neglects conservative contributions. The conservative contributions influence the motion only beyond the leading adiabatic order [8, 10, 11].

Important post-adiabatic effects can be found by continuing to neglect $g_\alpha^{(1)}$, but now integrating Eq. (1.2) using $G_i^{(1)}$ rather than its averaged variant. FH show that for “most” orbits, $G_i^{(1)}$ is given by $\langle G_i^{(1)} \rangle$ plus a rapidly oscillating contribution. Over the timescales associated with inspiral, this rapidly oscillating piece averages away and has little effect. The effect of the forcing term $G_i^{(1)}$ is dominated by $\langle G_i^{(1)} \rangle$ for “most” orbits.

However, for some orbits, this averaging fails. When $\Omega_\theta/\Omega_r = \beta_\theta/\beta_r$, where β_θ and β_r are small integers with no common factors, the contributions beyond $\langle G_i^{(1)} \rangle$ are *not* rapidly oscillating. Such “resonances” instead can importantly modify how the integrals of motion evolve during an inspiral. A given binary is very likely to evolve through several such resonances en route to the final merger of the smaller body with the large black hole. A complete quantitative understanding of these resonant effects will thus be quite important for making accurate inspiral models. Prior to FH’s analysis, several other papers argued that such resonances may play an important role in the radiative evolution of binary systems [12, 13] (albeit without quantifying the detailed impact they can

have), or else because of other effects which resonances have on the evolution of a dynamical system [14].

Orbits in which Ω_θ/Ω_r take on a small-integer ratio have been studied in great detail by Grossman, Levin, and Perez-Giz [15], who called them “periodic” orbits and provided a fairly simple scheme for classifying their features. They have also demonstrated that periodic orbits may play an important role in laying out a nearly optimal computational strategy for sampling the parameter space of large-mass ratio orbits more generally [16]. Following Ref. [9], we will call them “resonant” orbits, reflecting the fact that our main interest is in understanding how their periodic structure impacts the self interaction.

As a binary evolves through a resonance, its self interaction and thus its evolution are modified compared to what we would expect if the resonance were not taken into account. The details of how the self interaction is modified depend on the relative phase of the radial and angular motions as the orbit passes through resonance. Because of this, *resonances enhance the dependence of a binary’s orbital evolution on initial conditions*. Let the phase variable χ_0 define the value of the orbit’s θ angle at the moment it reaches periapsis (see Sec. II A for more details). On resonance, two orbits which have the same energy E , the same axial angular momentum L_z , and the same Carter constant Q will evolve differently if they have different values of χ_0 .

FH estimate [9] that the shift to the orbital phase induced by these resonances can be several tens to $\sim 10^2$ radians (as compared to an analysis which neglects the resonances). That there is such a large shift, and that this shift may depend on initial conditions, is potentially worrisome. Resonances could significantly complicate our ability to construct models for measuring the waves from extreme mass ratio inspirals. On the other hand, the detailed behavior of a system as it evolves through resonances may offer an opportunity to study an interesting aspect of strong-field gravity, providing a new handle for strong-gravity phenomenology.

The “several tens to $\sim 10^2$ radians” estimate is based on applying pN self force estimates to strong-field orbits, a regime where pN approximations are generally inaccurate. It is thus of great interest to estimate the impact of orbital resonances using strong-field methods. One can in fact compute the dissipative piece of the self force at leading order in the system’s mass ratio. Techniques for doing so with scalar fields were presented in Ref. [17]; generalizing to the gravitational dissipative self force is not terribly difficult [12, 13]. This computation uses solutions of the frequency-domain Teukolsky equation [18], which has been used in recent years most commonly to study “flux balancing” [19–21], the limit in which the driving force $G_i^{(1)}$ is replaced by its torus average $\langle G_i^{(1)} \rangle$.

A full analysis based on a strong-field dissipative self force is underway, and will be presented later. Our purpose here is to present a snapshot of the impact of resonances computed using strong-field techniques. In particular, we demonstrate how the phase-dependent effects

discovered by FH appear when an orbit is exactly on resonance, and we examine the numerical magnitude of the shift in the evolution of the integrals of motion due to this effect. In the language of Eq. (1.2), we compare the on-resonance rate of change of the integrals of motion with the rate we would obtain if we torus averaged the forcing term $G_i^{(1)}$.

We begin this paper by briefly reviewing the behavior of Kerr geodesic orbits in Sec. II. Much of this material has been presented elsewhere, so we leave out most details, pointing the reader to appropriate references. Our main focus is to describe how to find and characterize resonant orbits. We then describe how to compute radiation from Kerr orbits in Sec. III. We first briefly review the Teukolsky-equation-based formalism we use (Secs. III A – III C), and then describe how key details are modified by orbital resonances in Secs. III D and III E. We describe two complimentary approaches to computing fluxes on resonance. Although formally equivalent (as we prove in Appendix A), their implementation is quite different. Having both methods at hand proved useful to us in our numerical study. One aspect of the on-resonance computation (the evolution of Carter’s constant Q) is sufficiently complicated that all details of this calculation are given in Appendix B.

Our results are given in Sec. IV. We begin by examining how fluxes from individual modes (i.e., harmonics of the orbital frequencies) behave as a function of the offset phase of the radial and angular motions, χ_0 . We show that the amplitude of a given mode, and hence the rates of change of conserved quantities associated with that mode, can vary significantly with χ_0 . For example, the flux of energy from an orbit can vary by factors of order unity as χ_0 varies from 0 to 2π . The rate of change of the orbit’s Carter constant can even change sign as χ_0 varies. The total flux from a given orbit is given, however, by adding fluxes from many modes. When many modes are combined, much of the variation washes away; we find variations of a fraction of a percent in most quantities after summation. The amount of this residual variation seems to depend most strongly upon the geometry of the orbit’s (r, θ) motion on resonance, in particular the topology of the trace in the (r, θ) plane. Orbits whose motion in (r, θ) have a simple topology with few trajectory crossings in the plane (e.g., the $\Omega_\theta/\Omega_r = 3/2$ resonance) tend to have relatively large variation in the integrals of motion; orbits whose motion has a more complicated topology with many trajectory crossings show much less variation (e.g., the $\Omega_\theta/\Omega_r = 4/3$ resonance). We argue that this can be explained in terms of how the orbital motion tends (or fails) to average away variations in the source-term to the Teukolsky equation.

Understanding how these fluxes behave exactly on resonance is only the first step in building a complete strong-field understanding of how resonances impact inspirals. To go further, it will be necessary to examine how dissipation behaves as the system evolves up to and then through an orbital resonance. This analysis is just be-

ginning; we briefly outline the approach we are pursuing in Sec. V.

Throughout this paper, we use “relativist’s units,” setting $G = 1 = c$.

II. KERR GEODESICS AND ORBITAL RESONANCES

A. Brief summary of general characteristics

We begin by reviewing geodesic orbits of Kerr black holes, with a focus on aspects of this motion particularly relevant to our analysis. In most textbooks [for example, Ref. [22], Eqs. (33.32a)–(33.32d)], Kerr geodesics for a massive body are described using equations of motion in the Boyer-Lindquist coordinates t , r , θ , and ϕ :

$$\begin{aligned} \Sigma^2 \left(\frac{dr}{d\tau} \right)^2 &= [E(r^2 + a^2) - aL_z]^2 \\ &\quad - \Delta [r^2 + (L_z - aE)^2 + Q] \\ &\equiv R(r), \end{aligned} \quad (2.1)$$

$$\begin{aligned} \Sigma^2 \left(\frac{d\theta}{d\tau} \right)^2 &= Q - \cot^2 \theta L_z^2 - a^2 \cos^2 \theta (1 - E^2) \\ &\equiv \Theta(\theta), \end{aligned} \quad (2.2)$$

$$\begin{aligned} \Sigma \left(\frac{d\phi}{d\tau} \right) &= \csc^2 \theta L_z + aE \left(\frac{r^2 + a^2}{\Delta} - 1 \right) - \frac{a^2 L_z}{\Delta} \\ &\equiv \Phi(r, \theta), \end{aligned} \quad (2.3)$$

$$\begin{aligned} \Sigma \left(\frac{dt}{d\tau} \right) &= E \left[\frac{(r^2 + a^2)^2}{\Delta} - a^2 \sin^2 \theta \right] \\ &\quad + aL_z \left(1 - \frac{r^2 + a^2}{\Delta} \right) \\ &\equiv T(r, \theta). \end{aligned} \quad (2.4)$$

In these equations, τ is proper time along the geodesic, $\Sigma = r^2 + a^2 \cos^2 \theta$, and $\Delta = r^2 - 2Mr + a^2$. The quantities E and L_z are the orbital energy and axial angular momentum, normalized to the mass μ of the orbiting body, and Q is the orbit’s Carter constant, normalized to μ^2 . These three quantities are conserved on any geodesic.

Along with the coordinate time t and proper time τ , it is often very useful to work using a time parameter λ , defined by $d\lambda = d\tau/\Sigma$. The geodesic equations parameterized in this way are

$$\begin{aligned} \left(\frac{dr}{d\lambda} \right)^2 &= R(r), & \left(\frac{d\theta}{d\lambda} \right)^2 &= \Theta(\theta), \\ \frac{d\phi}{d\lambda} &= \Phi(r, \theta), & \frac{dt}{d\lambda} &= T(r, \theta). \end{aligned} \quad (2.5)$$

By using λ as our orbital parameter, the r and θ coordinate motions are completely separated from one another. Proper time τ couples r and θ by the factor Σ ; the coupling with coordinate time t is even more complicated. The parameter λ is often called “Mino time,” following Mino’s use of it to untangle these coordinate motions [11].

We have found it useful for many of our studies to introduce the following reparameterization of r and θ :

$$r = \frac{pM}{1 + e \cos \psi}, \quad \cos \theta = \cos \theta_m \cos(\chi + \chi_0). \quad (2.6)$$

These transformations replace the variables r and θ with secularly accumulating angles ψ and χ . As ψ and χ evolve from 0 to 2π , r and θ move through their full ranges of motion. We define $\chi = \psi = 0$ at $\lambda = 0$.

Notice that we include an offset phase χ_0 for the angular motion. We could also include an offset phase ψ_0 for the radial motion, as well as initial conditions ϕ_0 and t_0 for the ϕ and t coordinates. We choose our time origin such that $t = 0$ when $\lambda = 0$, which means $t_0 = 0$. We likewise choose $\phi_0 = 0$. Changing ϕ_0 is equivalent to rotating around the black hole's spin axis, and can have no effect on the flux of energy and angular momentum from the system (although it introduces a phase offset to the system's gravitational waves).

Finally, we choose $\psi_0 = 0$, which amounts to setting $\lambda = 0$ at a moment that the orbit passes through periapsis, $r = r_{\text{peri}} = pM/(1 + e)$. The offset phase χ_0 thus sets the value of θ at periapsis. Previous work (e.g., [19]) has typically used $\chi_0 = 0$ as well. The parameter set $(\psi_0, \chi_0, \phi_0, t_0)$ is equivalent to the set $(\lambda_0^r, \lambda_0^\theta, \phi_0, t_0)$ used in Ref. [17]. Following this reference, $\chi_0 = 0$ will label the “fiducial geodesic.” We will use it as a reference geodesic for some of the calculations in Sec. III.

In their original form, Eqs. (2.1) – (2.4), Kerr orbits are parameterized (up to initial conditions) by the three conserved constants E , L_z , and Q . The reparameterization (2.6) maps those constants to parameters that describes an orbit's coordinate geometry: semi-latus rectum p , eccentricity e , and minimum angle θ_m . These quantities are likewise conserved along a geodesic. Schmidt [23] provides closed-form expressions for converting between (E, L_z, Q) and (p, e, θ_m) . Either the set (E, L_z, Q) or (p, e, θ_m) , plus the relative phase χ_0 , completely specifies a geodesic for our purposes here.

B. Orbital frequencies and resonances

Each orbit has a unique set of frequencies describing its motions with respect to r , θ , and ϕ . The frequencies

$$\Omega_{r,\theta,\phi} = 2\pi/T_{r,\theta,\phi} \quad (2.7)$$

are conjugate to the periods¹ expressed in coordinate time t ; the frequencies

$$\Upsilon_{r,\theta,\phi} = 2\pi/\Lambda_{r,\theta,\phi} \quad (2.8)$$

are conjugate to these periods in Mino time λ . These two frequencies are related by a factor Γ which describes the average increase in t per unit λ :

$$\Omega_{r,\theta,\phi} = \Upsilon_{r,\theta,\phi}/\Gamma. \quad (2.9)$$

Details of how to compute Γ given (E, L_z, Q) or (p, e, θ_m) are given in Ref. [24]. One could also define frequencies conjugate to proper time τ (see, e.g., Ref. [23] and discussion in Sec. I), but the Ω and Υ frequencies will be sufficient for our purposes.

As background to Sec. III, we compare a typical orbit, for which the ratio Ω_θ/Ω_r is some irrational number, to a resonant orbit, for which $\Omega_\theta/\Omega_r = \beta_\theta/\beta_r$, where β_θ and β_r are small integers with no common factors. Figure 1 shows the motion of three orbits, projected into the (r, θ) plane. In all cases, we have chosen $p = 3.2758$, $e = 0.7$, $\theta_m = 70^\circ$; the motion is thus bound to the range $1.93M \leq r \leq 10.9M$, $70^\circ \leq \theta \leq 110^\circ$.

In the right-hand panel, we have set the spin parameter $a = 0.95M$. For these orbital parameters, this orbit has $\Omega_\theta/\Omega_r = 2.0311\dots$. This is *not* a resonant orbit; notice that the roughly nine radial periods shown here do not close. The orbital trace in this case ergodically fills the (r, θ) plane. In the left-hand panel, we have set $a = 0.9M$, which yields $\Omega_\theta/\Omega_r = 3$ — these orbits are in a 3:1 resonance. The two traces shown in this panel correspond to different choices of χ_0 . The green trace has $\chi_0 = 0$ (so that $\theta = \theta_m = 70^\circ$ at periapsis), and the red trace has $\chi_0 = \pi/2$ (so that $\theta = 90^\circ$ at periapsis). Both traces show roughly nine complete radial periods. By their periodic nature, their motion traces out Lissajous figures: No matter how long we follow these orbits, they trace out a 1-dimensional trajectory in the (r, θ) plane.

Note that the geometry of the traces in the left-hand panel varies significantly as χ_0 is varied. The topology of these traces remains fixed, however: In all cases the trace oscillates three times in the angular direction as it completes a single radial oscillation. As emphasized by Grossman et al. [15], the topology of resonant orbits is uniquely determined by their orbital parameters, by virtue of the integers β_θ and β_r that determine their periodicity. We show some evidence in Sec. IV that the topology of resonant orbits directly affects the strength of their resonance. Simple orbits, which do not cross themselves often and do not “cover” much of the allowed (r, θ) plane, show large variations in their radiated fluxes as the phase χ_0 is varied; more complicated orbits, which cross themselves many times and come “close to” much of the allowed (r, θ) plane, do not show such large variations.

III. GRAVITATIONAL RADIATION FROM KERR ORBITS

Here we describe in detail how we compute radiation from strong-field orbits, with an emphasis on how resonances modify the “usual” behavior. We begin in Sec.

¹ Describing the periods using Boyer-Lindquist time t is a bit complicated; $T_{r,\theta,\phi}$ really describe an averaged notion of the periods. See Refs. [23, 24] for more detailed discussion.

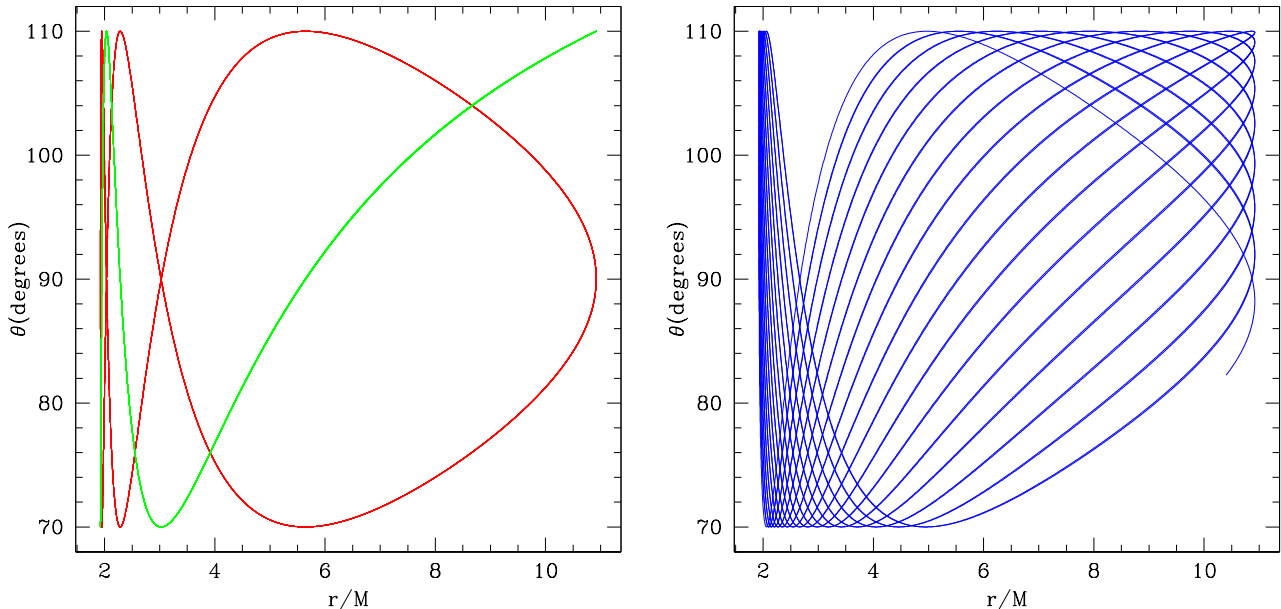


FIG. 1: Left: Lissajous figures describing motion in the (r, θ) plane on a 3:1 orbital resonance ($a = 0.9M$, $p = 3.2758M$, $e = 0.7$, $\theta_m = 70^\circ$). The green trace has $\theta = \theta_m$ at periastris; red has $\theta = \pi/2$ at periastris. Approximately nine radial cycles are used to generate these traces. Right: Ergodic motion of a “normal” orbit. The orbit’s geometry is identical to that in the left-hand panel, but we have changed the black hole’s spin to $a = 0.95M$; this changes the ratio of frequencies to $\Omega_\theta/\Omega_r = 2.0311\dots$. Again, roughly nine radial cycles are shown here. Given enough time, the blue trace would pass arbitrarily close to all points in $70^\circ \leq \theta \leq 110^\circ$, $2M \lesssim r \lesssim 12M$.

III A by briefly reviewing the Teukolsky equation and its solutions. This material has been presented at length in several other papers, so we only give a summary. Our goal is to provide just enough detail to understand how the situation changes on resonance. Section III B describes how to compute fluxes of energy E and angular momentum L_z from Teukolsky equation solutions, highlighting how this calculation must be modified for resonant orbits. The analogous calculation for the Carter constant calculation is sufficiently complicated that we present its details in Appendix B, with a summary in Sec. III C. Finally, Secs. III D and III E present two different ways to compute on-resonant fluxes. These methods are equivalent to one another, although their computational implementations are quite different.

A. The frequency-domain Teukolsky equation and its solutions

Our computation of the small body’s self interaction uses the Teukolsky equation [18]. This equation governs the radiative components to a Kerr black hole’s spacetime curvature, ψ_0 and ψ_4 , which arise due to some perturbing source or field. In the relevant limits, identities make it possible to obtain all information about the field ψ_0 from ψ_4 , and vice versa, so we need only focus on one. The field ψ_4 is particularly convenient for describing radiation

at infinity.

Teukolsky showed [18] that, imposing the Fourier and multipolar decomposition

$$\psi_4 = \rho^4 \int_{-\infty}^{\infty} d\omega \sum_{lm} R_{lm\omega}(r) S_{lm\omega}(\theta) e^{i(m\phi - \omega t)}, \quad (3.1)$$

where $\rho = -1/(r - ia \cos \theta)$, a master partial differential equation governing ψ_4 separates. The function $S_{lm\omega}(\theta)$ is a spin-weighted spheroidal harmonic; Ref. [25] presents techniques for computing it to high accuracy. The radial function is governed by

$$\Delta^2 \frac{d}{dr} \left(\frac{1}{\Delta} \frac{dR_{lm\omega}}{dr} \right) - V(r) R_{lm\omega} = -\mathcal{T}_{lm\omega}(r, \chi_0). \quad (3.2)$$

Equation (3.2) is the Teukolsky equation (although that name is also used for the PDE that governs ψ_4 before separating variables). Setting the right-hand side of (3.2) to zero, we construct a pair of homogeneous solutions, $R_{lm\omega}^H$ (which is regular on the event horizon) and $R_{lm\omega}^\infty$ (which is regular at infinity). See Ref. [19] (hereafter DH06) for detailed discussion of how we construct these solutions, as well as for the potential $V(r)$ appearing in Eq. (3.2). From these solutions, it is straightforward to build a Green’s function which can then be integrated over the source $\mathcal{T}_{lm\omega}$ to construct a particular solution.

The source $\mathcal{T}_{lm\omega}$ is sufficiently complicated that we will not write it out explicitly; see DH06 for details. It is built

from projections of the stress-energy tensor for a small body orbiting the black hole,

$$T_{\alpha\beta} = \frac{\mu u_\alpha u_\beta}{\Sigma \sin \theta dt/d\tau} \delta[r - r_o(t)] \delta[\theta - \theta_o(t, \chi_0)] \delta[\phi - \phi_o(t)], \quad (3.3)$$

where μ is the mass of the small body, and u_α are the components of its orbital 4-velocity. The subscript “o” on the coordinates in the delta functions stands for “orbit,” labeling the orbit’s coordinates (as opposed to a general field point, which we leave without a subscript).

Note that $\mathcal{T}_{lm\omega}$ is a frequency-domain quantity. Because it arises from Kerr orbital motion, it only has support at frequencies $\omega_{mkn} = m\Omega_\phi + k\Omega_\theta + n\Omega_r$, and is non-zero only for $r_{\min} \leq r \leq r_{\max}$, $\theta_m \leq \theta \leq \pi - \theta_m$ [where $r_{\min} = p/(1+e)$, and $r_{\max} = p/(1-e)$; see Eq. (2.6)]. Once fully constructed, $\mathcal{T}_{lm\omega}$ has terms in $\delta[r - r_o(t)]$ and its first two radial derivatives; see Sec. III of DH06.

To understand fluxes from this system, our interest is in $R_{lm\omega}(r)$ in the limits $r \rightarrow \infty$ and $r \rightarrow r_+$ (the event horizon). These limits will allow us to deduce how the orbit evolves due to radiation to infinity, and due to radiation absorbed by the hole. As $r \rightarrow \infty$, the homogeneous solution $R_{lm\omega}^\infty(r)$ approaches (modulo a power-law scaling) an outgoing plane wave. Likewise, as $r \rightarrow r_+$, the solution $R_{lm\omega}^H(r)$ limits to an ingoing plane wave. The particular solution we construct by integrating the Green’s function over the source then takes the form

$$R_{lm\omega}(r) = \begin{cases} Z_{\omega lm}^H(\chi_0) R_{\omega lm}^\infty(r) & r \rightarrow \infty, \\ Z_{\omega lm}^\infty(\chi_0) R_{\omega lm}^H(r) & r \rightarrow r_+, \end{cases} \quad (3.4)$$

where

$$Z_{lm\omega}^\star(\chi_0) = C^\star \int_{r_+}^\infty dr' \frac{R_{lm\omega}^\star(r') \mathcal{T}_{lm\omega}(r', \chi_0)}{\Delta(r')^2}, \quad (3.5)$$

and where \star can stand for ∞ or H . The symbol C^\star is shorthand for a collection of constants whose value is not needed here; see Sec. III of DH06 for further discussion.

Next insert $\mathcal{T}_{lm\omega}$ into Eq. (3.5) and perform the r integral. The result is a Fourier transform:

$$\begin{aligned} Z_{lm\omega}^\star(\chi_0) &= C^\star \int_{-\infty}^\infty dt e^{i[\omega t - \phi(t)]} I_{lm\omega}^\star[r_o(t), \theta_o(t, \chi_0)] \\ &= C^\star \int_{-\infty}^\infty d\lambda e^{i(\omega \Gamma - m \Upsilon_\phi) \lambda} \times \\ &\quad J_{lm\omega}^\star[r_o(\lambda), \theta_o(\lambda, \chi_0)]. \end{aligned} \quad (3.6)$$

The function $I_{lm\omega}^\star$ introduced on the first line of Eq. (3.6) is built from $\mathcal{T}_{lm\omega}$; see Eqs. (3.30)–(3.33) in DH06 and associated text for detailed discussion. On the second line, we have changed the integration variable from coordinate time t to Mino time λ , and defined

$$J_{lm\omega}^\star(r_o, \theta_o) = I_{lm\omega}^\star(r_o, \theta_o) T(r_o, \theta_o) \times e^{i[\omega \Delta t(r_o, \theta_o) - m \Delta \phi(r_o, \theta_o)]}. \quad (3.7)$$

[In any place that we indicate a dependence on (r_o, θ_o) , please note that this is shorthand for $[r_o(\lambda), \theta_o(\lambda, \chi_0)]$.] The function $J_{lm\omega}^\star(r_o, \theta_o)$ is just $I_{lm\omega}^\star(r_o, \theta_o)$ reweighted by $T(r_o, \theta_o)$ [the right-hand side of the geodesic equation (2.4)], and with the factor $e^{i(\omega \Delta t - m \Delta \phi)}$ included. The functions $\Delta t(r_o, \theta_o)$ and $\Delta \phi(r_o, \theta_o)$ are oscillatory contributions to the t and ϕ pieces of the orbit:

$$t_o(\lambda) = \Gamma \lambda + \Delta t[r_o(\lambda), \theta_o(\lambda, \chi_0)], \quad (3.8)$$

$$\phi_o(\lambda) = \Upsilon_\phi \lambda + \Delta \phi[r_o(\lambda), \theta_o(\lambda, \chi_0)]. \quad (3.9)$$

Both Δt and $\Delta \phi$ oscillate at harmonics of Υ_θ and Υ_r ; see Ref. [24] for detailed discussion.

The function $J_{lm\omega}^\star(r_o, \theta_o)$ gathers all the pieces of the integrand for $Z_{lm\omega}^\star$ that can be described as harmonics of Υ_θ and Υ_r . As such, it is useful to decompose it into these harmonics:

$$J_{lm\omega}^\star(r_o, \theta_o) = \sum_{kn} J_{\omega lmkn}^\star(\chi_0) e^{-i(k \Upsilon_\theta + n \Upsilon_r) \lambda}, \quad (3.10)$$

where

$$\begin{aligned} J_{\omega lmkn}^\star(\chi_0) &= \frac{\Upsilon_r \Upsilon_\theta}{(2\pi)^2} \int_0^{2\pi/\Upsilon_\theta} d\lambda^\theta \int_0^{2\pi/\Upsilon_r} d\lambda^r \\ &\quad e^{i(k \Upsilon_\theta \lambda^\theta + n \Upsilon_r \lambda^r)} J_{lm\omega}^\star[r_o(\lambda^r), \theta_o(\lambda^\theta, \chi_0)]. \end{aligned} \quad (3.11)$$

We have here taken advantage of the fact that Mino time completely decouples the r and θ motions from one another. We imagine that these two coordinates depend separately on two different Mino-time variables, λ^r and λ^θ , and integrate over a full period of each time. See Ref. [24] for detailed discussion of this trick.

Next, combine Eqs. (3.6), (3.7), (3.10), and (3.11) to find

$$\begin{aligned} Z_{lm\omega}^\star(\chi_0) &= \frac{2\pi}{\Gamma} \sum_{kn} J_{\omega lmkn}^\star(\chi_0) \delta(\omega - \omega_{mkn}) \\ &\equiv \sum_{kn} Z_{lmkn}^\star(\chi_0) \delta(\omega - \omega_{mkn}). \end{aligned} \quad (3.12)$$

On the last line, we have taken advantage of the fact that the delta functions mean that the RHS only has support at $\omega = \omega_{mkn}$, and we have defined

$$\begin{aligned} Z_{\omega lmkn}^\star(\chi_0) &= \frac{2\pi}{\Gamma} J_{\omega lmkn}^\star(\chi_0) \\ &= \frac{\Upsilon_r \Upsilon_\theta}{2\pi \Gamma} \int_0^{2\pi/\Upsilon_\theta} d\lambda^\theta \int_0^{2\pi/\Upsilon_r} d\lambda^r \\ &\quad e^{i(k \Upsilon_\theta \lambda^\theta + n \Upsilon_r \lambda^r)} J_{lm\omega}^\star[r_o(\lambda^r), \theta_o(\lambda^\theta, \chi_0)] \end{aligned} \quad (3.13)$$

and

$$Z_{lmkn}^\star(\chi_0) = Z_{\omega_{mkn} lmkn}^\star(\chi_0). \quad (3.15)$$

Throughout this synopsis, we have explicitly shown the dependence on the relative phase χ_0 . To account for its influence on the amplitudes, let us first define

$$\check{Z}_{lmkn}^* \equiv Z_{lmkn}^*(\chi_0 = 0) . \quad (3.16)$$

In other words, amplitudes with a check mark $\check{\cdot}$ are computed using the fiducial geodesic. As shown in Sec. 8.4 of Ref. [17], the effect of χ_0 is to introduce a phase:

$$Z_{lmkn}^*(\chi_0) = e^{i\xi_{mkn}(\chi_0)} \check{Z}_{lmkn}^* , \quad (3.17)$$

where

$$\xi_{mkn}(\chi_0) = k\Upsilon_\theta \lambda_0^\theta + m\Delta\hat{\phi}[r_{\min}, \theta(-\lambda_0^\theta)] - \omega_{mkn}\Delta\hat{t}[r_{\min}, \theta(-\lambda_0^\theta)] , \quad (3.18)$$

where $\Delta\hat{\phi}$ is $\Delta\phi$ for the fiducial geodesic (and likewise for $\Delta\hat{t}$), and where $\lambda_0^\theta = \lambda_0^\theta(\chi_0)$ is the value of λ^θ at which $\theta = \theta_m$. It is given explicitly by Eq. (3.75) of Ref. [17]. On the fiducial geodesic, $\lambda_0^\theta = 0$, and $\xi_{mkn} = 0$, as it should.

B. Non-resonant fluxes of energy and angular momentum

Once the coefficients $Z_{lmkn}^*(\chi_0)$ are computed, it is straightforward to compute the fluxes of energy and angular momentum to infinity and down the black hole's event horizon. In this section, we present in some detail the calculation of fluxes to infinity, in order to highlight the step of the calculation which changes for radiation from resonant orbits. Resonance changes the down-horizon fluxes in exactly the same way. Since the down-horizon calculation is more complicated, we do not go through it in detail, but just summarize the final result.

Using Eq. (3.1) and the definitions which follow, we find that as $r \rightarrow \infty$,

$$\begin{aligned} \psi_4 &= \frac{1}{r} \sum_{lmkn} e^{i\xi_{mkn}(\chi_0)} \check{Z}_{lmkn}^H S_{lmkn}(\theta) e^{i(m\phi - \omega_{mkn}t)} \\ &\equiv \frac{1}{r} \sum_{lmkn} \psi_{4,lmkn} . \end{aligned} \quad (3.19)$$

Here, $S_{lmkn}(\theta)$ is the spheroidal harmonic $S_{lm\omega}(\theta)$ for $\omega = \omega_{mkn}$. As $r \rightarrow \infty$, $\psi_4 \rightarrow (1/2)(\ddot{h}_+ - i\ddot{h}_\times)$. This means that

$$h_+ - ih_\times = -\frac{2}{r} \sum_{lmkn} \frac{\psi_{4,lmkn}}{\omega_{mkn}^2} . \quad (3.20)$$

A very useful tool for understanding the energy carried by gravitational waves is the Isaacson stress-energy tensor [26],

$$\begin{aligned} T_{\mu\beta}^{\text{rad}} &= \frac{1}{16\pi} \langle \nabla_\mu h_+ \nabla_\beta h_+ + \nabla_\mu h_\times \nabla_\beta h_\times \rangle \\ &\simeq \frac{1}{16\pi} \langle \partial_\mu h_+ \partial_\beta h_+ + \partial_\mu h_\times \partial_\beta h_\times \rangle . \end{aligned} \quad (3.21)$$

The angle brackets mean that the quantity must be averaged over several wavelengths; see Ref. [26] and references therein for detailed discussion of the averaging procedure necessary for $T_{\mu\beta}^{\text{rad}}$ to be a proper tensor to the relevant order. On the first line, ∇_μ denotes a covariant derivative with respect to the background; on the second line, we take advantage of the fact that this limits to the partial derivative as $r \rightarrow \infty$.

The energy flux, our focus here, is given by

$$\begin{aligned} \frac{dE^\infty}{dt} &= \lim_{r \rightarrow \infty} r^2 \int T_{tk}^{\text{rad}} n^k d\Omega \\ &= \lim_{r \rightarrow \infty} r^2 \int T_{tt}^{\text{rad}} d\Omega , \end{aligned} \quad (3.22)$$

where n^k is a radially outward pointing normal vector, and the index k is restricted to spatial directions.

Combining Eqs. (3.20) – (3.22), we find

$$\left\langle \frac{dE^\infty}{dt} \right\rangle = \left\langle \sum_{lmkn} \sum_{l'm'k'n'} \text{Re} \int \frac{\psi_{4,lmkn} \bar{\psi}_{4,l'm'k'n'}}{4\pi\omega_{mkn}\omega_{m'k'n'}} d\Omega \right\rangle ; \quad (3.23)$$

$\bar{\psi}_4$ is the complex conjugate of ψ_4 . The sum over l is taken from 2 to ∞ ; the sum over m from $-l$ to l ; and the sums over k and n are both taken from $-\infty$ to ∞ . Similar rules apply to the sum over primed indices. The angle brackets on the left-hand side mean that this rate of change is to be understood as one which is averaged over appropriate orbital timescales.

Consider now averaging the right-hand side over several wavelengths. Assuming that each frequency ω_{mkn} is distinct (an assumption that is only true when we are not on a resonance), then this averaging forces $m = m'$, $k = k'$, $n = n'$. Using the fact that

$$\int S_{lmkn}(\theta) S_{l'mkn}(\theta) d\Omega = \delta_{ll'} , \quad (3.24)$$

we find

$$\left\langle \frac{dE^\infty}{dt} \right\rangle = \sum_{lmkn} \frac{|\check{Z}_{lmkn}^H|^2}{4\pi\omega_{mkn}^2} \equiv \sum_{lmkn} \dot{E}_{lmkn}^\infty . \quad (3.25)$$

A similar calculation focusing on $T_{t\phi}^{\text{rad}}$ gives us the flux of axial angular momentum:

$$\left\langle \frac{dL_z^\infty}{dt} \right\rangle = \sum_{lmkn} \frac{m|\check{Z}_{lmkn}^H|^2}{4\pi\omega_{mkn}^3} \equiv \sum_{lmkn} \dot{L}_{lmkn}^\infty . \quad (3.26)$$

Notice that the phase ξ_{mkn} does not appear in Eqs. (3.25) and (3.26).

The calculation of fluxes down the horizon is more complicated. The Isaacson tensor is not defined in a black hole's strong field. Instead, one must use the fact that the curvature perturbation due to the orbiting body exerts a shear on the generators of the horizon, which increases the black hole's surface area. By the first law of black hole dynamics, this in turn changes its mass and

angular momentum; see Refs. [27, 28] for detailed discussion. Assuming flux balance, we can then read out the down-horizon fluxes:

$$\left\langle \frac{dE^H}{dt} \right\rangle = \sum_{lmkn} \alpha_{lmkn} \frac{|\check{Z}_{lmkn}^\infty|^2}{4\pi\omega_{mkn}^2} \equiv \sum_{lmkn} \dot{E}_{lmkn}^H, \quad (3.27)$$

$$\left\langle \frac{dL_z^H}{dt} \right\rangle = \sum_{lmkn} \alpha_{lmkn} \frac{m|\check{Z}_{lmkn}^\infty|^2}{4\pi\omega_{mkn}^3} \equiv \sum_{lmkn} \dot{L}_{z,lmkn}^H. \quad (3.28)$$

We refer the reader to Eq. (3.60) of DH06 for the down-horizon factor α_{lmkn} .

C. Non-resonant rate of change of the Carter constant

The Carter constant Q is the third integral which allows one to separate the equations of motion for orbits of Kerr black holes. Unlike the energy and axial angular momentum, there is no simple formula describing the “flux” of Carter constant carried by radiation. However, one can formulate how Q changes due to radiative back-reaction. Taking into account only the dissipative piece of the self force and averaging over very long times, Sago et al. [21] (hereafter S06) showed that

$$\begin{aligned} \left\langle \frac{dQ^\infty}{dt} \right\rangle &= \sum_{lmkn} |\check{Z}_{lmkn}^H|^2 \times \frac{(\mathcal{L}_{mkn} + k\Upsilon_\theta)}{2\pi\omega_{mkn}^3}, \quad (3.29) \\ \left\langle \frac{dQ^H}{dt} \right\rangle &= \sum_{lmkn} \alpha_{lmkn} |\check{Z}_{lmkn}^\infty|^2 \times \frac{(\mathcal{L}_{mkn} + k\Upsilon_\theta)}{2\pi\omega_{mkn}^3}, \quad (3.30) \end{aligned}$$

where

$$\mathcal{L}_{mkn} = m\langle \cot^2 \theta \rangle L_z - a^2 \omega_{mkn} \langle \cos^2 \theta \rangle E. \quad (3.31)$$

It is interesting that the rate of change of Q can be factored into quantities that are encoded in the distant radiation (\check{Z}_{lmkn}^H and \check{Z}_{lmkn}^∞) and quantities that are local to the orbital worldline (\mathcal{L}_{mkn} , ω_{mkn} , and Υ_θ). Using Eqs. (3.25) and (3.27), these results can be written

$$\left\langle \frac{dQ^\star}{dt} \right\rangle = 2 \sum_{lmkn} \dot{E}_{lmkn}^\star \times (\mathcal{L}_{mkn} + k\Upsilon_\theta) / \omega_{mkn}, \quad (3.32)$$

where \star is either ∞ or H . We go through the Sago et al. calculation of $\langle dQ/dt \rangle$ in some detail in Appendix B in order to understand how to modify this result on an orbital resonance.

Note that the rates of change $\langle dE^\star/dt \rangle$, $\langle dL_z^\star/dt \rangle$, and $\langle dQ^\star/dt \rangle$ are equivalent for non-resonant orbits to the three components of the torus-averaged forcing term $\langle G_i^{(1)} \rangle$ introduced in the introduction, albeit using coordinate time t rather than proper time τ to parameterize the rate of change. This equivalence breaks down for resonant orbits.

D. Radiation from resonant orbits I: Merging of amplitudes on resonance

On resonance, $\Omega_\theta/\beta_\theta = \Omega_r/\beta_r \equiv \Omega$, and so $k\Omega_\theta + n\Omega_r = N\Omega$, where $N = k\beta_\theta + n\beta_r$. An infinite number of pairs (k, n) are consistent with a given N . For a given value of m , all pairs (k, n) satisfying $k\beta_\theta + n\beta_r = N$ will have mode frequency $\omega_{mkn} \equiv \omega_{mN} = m\Omega_\phi + N\Omega$.

Revisiting Eq. (3.19), this means that only three indices are needed to describe the radiation on resonance, rather than four:

$$\psi_4^{\text{res}} = \frac{1}{r} \sum_{lmN} \mathcal{Z}_{lmN}^H(\chi_0) S_{lmN}(\theta) e^{i(m\phi - \omega_{mN}t)}, \quad (3.33)$$

where

$$\mathcal{Z}_{lmN}^\star(\chi_0) = \sum_{(k,n)_N} e^{i\xi_{mkn}(\chi_0)} \check{Z}_{lmkn}^\star, \quad (3.34)$$

and where $(k, n)_N$ denotes all pairs (k, n) which satisfy $k\beta_\theta + n\beta_r = N$. In Eq. (3.33), the sums over l and m are exactly as before, and N is summed from $-\infty$ to ∞ .

Equations (3.33) and (3.34) tell us that, as we enter a resonance, modes of ψ_4 which were distinct combine with one another: “lines” in the gravitational-wave spectrum merge. Each mode’s contribution to the combined amplitude (3.34) is weighted by its phase $\xi_{mkn}(\chi_0)$. Revisiting the calculation of the fluxes using Eq. (3.33) rather than (3.19), we find

$$\begin{aligned} \left\langle \frac{dE^\infty}{dt}(\chi_0) \right\rangle &= \sum_{lmN} \frac{|\mathcal{Z}_{lmN}^H(\chi_0)|^2}{4\pi\omega_{mN}^2} \\ &\equiv \sum_{lmN} \dot{E}_{lmN}^\infty(\chi_0), \quad (3.35) \end{aligned}$$

$$\begin{aligned} \left\langle \frac{dE^H}{dt}(\chi_0) \right\rangle &= \sum_{lmN} \alpha_{lmN} \frac{|\mathcal{Z}_{lmN}^\infty(\chi_0)|^2}{4\pi\omega_{mN}^2} \\ &\equiv \sum_{lmN} \dot{E}_{lmN}^H(\chi_0), \quad (3.36) \end{aligned}$$

$$\begin{aligned} \left\langle \frac{dL_z^\infty}{dt}(\chi_0) \right\rangle &= \sum_{lmN} \frac{m|\mathcal{Z}_{lmN}^\infty(\chi_0)|^2}{4\pi\omega_{mN}^3} \\ &\equiv \sum_{lmN} \dot{L}_{z,lmN}^\infty(\chi_0), \quad (3.37) \end{aligned}$$

$$\begin{aligned} \left\langle \frac{dL_z^H}{dt}(\chi_0) \right\rangle &= \sum_{lmN} \alpha_{lmN} \frac{m|\mathcal{Z}_{lmN}^\infty(\chi_0)|^2}{4\pi\omega_{mN}^3} \\ &\equiv \sum_{lmN} \dot{L}_{z,lmN}^H(\chi_0). \quad (3.38) \end{aligned}$$

(The factor α_{lmN} appearing here is the same as α_{lmkn} introduced earlier, but with ω_{mkn} replaced by ω_{mN} .) Thanks to the dependence of \mathcal{Z}_{lmN}^\star on the relative phase χ_0 , the on-resonance fluxes likewise depend on this phase.

In Appendix B, we show how the calculation of dQ/dt

is changed due to an orbital resonance. The result is

$$\left\langle \frac{dQ^\infty}{dt}(\chi_0) \right\rangle = \sum_{lmN} \frac{|\mathcal{Z}_{lmN}^H(\chi_0)|^2}{2\pi\omega_{mN}^3} \mathcal{L}_{mN} + \Upsilon_\theta \sum_{lmN} \frac{\text{Re} [\mathcal{Z}_{lmN}^H(\chi_0) \bar{\mathcal{Y}}_{lmN}^H(\chi_0)]}{2\pi\omega_{mN}^3}, \quad (3.39)$$

$$\left\langle \frac{dQ^H}{dt}(\chi_0) \right\rangle = \sum_{lmN} \frac{\alpha_{lmN} |\mathcal{Z}_{lmN}^\infty(\chi_0)|^2}{2\pi\omega_{mN}^3} \mathcal{L}_{mN} + \Upsilon_\theta \sum_{lmN} \frac{\alpha_{lmN} \text{Re} [\mathcal{Z}_{lmN}^\infty(\chi_0) \bar{\mathcal{Y}}_{lmN}^\infty(\chi_0)]}{2\pi\omega_{mN}^3}. \quad (3.40)$$

The factor \mathcal{L}_{mN} is the same as \mathcal{L}_{mkn} with ω_{mkn} replaced by ω_{mN} . We have introduced the modified amplitude

$$\mathcal{Y}_{lmN}^*(\chi_0) = \sum_{(k,n)_N} k e^{i\xi_{mkn}(\chi_0)} \tilde{Z}_{lmkn}^*. \quad (3.41)$$

Notice that $\mathcal{Y}_{lmN}^*(\chi_0)$ is similar to $\mathcal{Z}_{lmN}^*(\chi_0)$ [compare Eq. (3.34)], but with each term in the sum weighted by k . Equations (3.39) and (3.40) are used in the following section to study how the Carter constant's evolution is affected by an orbital resonance.

E. Radiation from resonant orbits II: The constrained source integral of a resonant orbit

The method described in Sec. IIID builds the on-resonance amplitudes $\mathcal{Z}_{lmN}^*(\chi_0)$ from the amplitudes \tilde{Z}_{lmkn}^* which are normally computed with frequency-domain Teukolsky equation solvers, such as that described in DH06. The only modification is the need to compute the phase $\xi_{mkn}(\chi_0)$.

One can also compute the on-resonant amplitudes by modifying the integral for the amplitudes \tilde{Z}_{lmkn}^* . Doing so, we compute $\mathcal{Z}_{lmN}^*(\chi_0)$ directly, without reference to the amplitudes \tilde{Z}_{lmkn}^* . We begin this calculation by carrying over without modification the computation of Sec. III A up to Eq. (3.6),

$$Z_{lm\omega}^* = C^* \int_{-\infty}^{\infty} d\lambda e^{i(\omega\Gamma - m\Upsilon_\phi)\lambda} J_{lm\omega}^*[r_o(\lambda), \theta_o(\lambda, \chi_0)].$$

As before, we decompose $J_{lm\omega}^*$ into Υ_θ and Υ_r harmonics. However, we now take into account how these frequencies are related on a resonance:

$$\begin{aligned} J_{lm\omega}^* &= \sum_{kn} J_{\omega lmkn}^* e^{-i(k\Upsilon_\theta + n\Upsilon_r)\lambda} \\ &= \sum_{kn} J_{\omega lmkn}^* e^{-i(k\beta_\theta + n\beta_r)\Upsilon\lambda} \\ &\equiv \sum_N \mathcal{J}_{\omega lmN}^* e^{-iN\Upsilon\lambda}. \end{aligned} \quad (3.42)$$

On the second line, we've used the resonance relation $\Upsilon_\theta/\beta_\theta = \Upsilon_r/\beta_r \equiv \Upsilon$. We then use $N = k\beta_\theta + n\beta_r$, and change notation slightly to distinguish the source amplitude $J_{\omega lmkn}^*$ from its on-resonance variant $\mathcal{J}_{\omega lmN}^*$.

The result, Eq. (3.42), depends on only one fundamental frequency, Υ . As such, our integral for $\mathcal{J}_{\omega lmN}^*$ is taken over only a single time variable λ :

$$\mathcal{J}_{\omega lmN}^*(\chi_0) = \frac{\Upsilon}{2\pi} \int_0^{2\pi/\Upsilon} d\lambda J_{lm\omega}^*[r_o(\lambda), \theta_o(\lambda, \chi_0)] e^{iN\Upsilon\lambda}. \quad (3.43)$$

Finally, by combining Eqs. (3.6), (3.7), (3.42), and (3.43), we define

$$\mathcal{Z}_{lmN}^*(\chi_0) = \frac{2\pi}{\Gamma} \mathcal{J}_{\omega_{mN} lmN}^*(\chi_0) \quad (3.44)$$

$$= \frac{\Upsilon}{\Gamma} \int_0^{2\pi/\Upsilon} d\lambda J_{lm\omega_{mN}}^*[r(\lambda), \theta(\lambda, \chi_0)] e^{iN\Upsilon\lambda}. \quad (3.45)$$

In combining these equations, we find a proportionality to $\delta(\omega - \omega_{mN})$, which forces the RHS to have support only at $\omega = \omega_{mN}$. Although it may not be obvious, Eqs. (3.34) and (3.45) are equivalent. We show this analytically in Appendix A, and will demonstrate it numerically in the following section. A conceptually attractive feature of Eq. (3.45) is that the integrand is only evaluated at the coordinates (r, θ) which the on-resonance orbit passes through. Changing χ_0 changes the points (r, θ) at which the integrand has support. This is how the dependence on χ_0 enters \mathcal{Z}_{lmN}^* in this calculation.

However, Eq. (3.45) can only be used for orbits that are *exactly* on resonance. Indeed, in any other case, the 3-index amplitude \mathcal{Z}_{lmN}^* is not meaningful since the on-resonance condition $k\beta_\theta + n\beta_r = N$ is not met. A suitable generalization of Eq. (3.34) for slightly off-resonance orbits can be used to understand the behavior of ψ_4 as one approaches and moves through a resonance. As such, the sum of phase-weighted amplitudes, Eq. (3.34), is likely to be more useful for understanding the resonant self interaction in full inspiral studies. In any case, we have found having two techniques for computing $\mathcal{Z}_{lmN}^*(\chi_0)$ to be very useful. The codes which implement these two formulae are quite different, so it is reassuring that their results are in agreement. As discussed at the end of Appendix B, it appears that the modified amplitude $\mathcal{Y}_{lmN}(\chi_0)$ can also be computed with a one dimensional integral by propagating the operator $(d\theta/d\lambda)\partial_\theta$ under the integral in Eq. (3.45). We have not yet tested this, though it would be a worthwhile exercise to do so.

IV. RESULTS: HOW RESONANCES IMPACT RADIATION

A. Variation of modes with χ_0 , and comparison of two computational techniques

We now discuss examples illustrating how wave amplitudes and fluxes are affected by orbital resonances. All of our results are computed using a version of the code described in DH06, modified to handle resonances.

Begin with Fig. 2, which illustrates how \mathcal{Z}_{lmN}^H and \mathcal{Z}_{lmN}^∞ behave as functions of χ_0 . For this example, we have put $a = 0.9M$, $p = 8.7744M$, $e = 0.7$, $\theta_m = 20^\circ$ (for which $\Omega_\theta/\Omega_r = 3/2$), and we have chosen $l = 4$, $m = 3$, $N = 7$. In all panels, the green curves show \mathcal{Z}_{lmN}^* computed using Eq. (3.34); the red dots show the same quantity computed using Eq. (3.45). The two methods agree to numerical accuracy (roughly 6 digits²). All examples that we have examined show that Eqs. (3.34) and (3.45) agree perfectly (as we would expect from the calculation presented in Appendix A). Having both methods at hand was quite useful for debugging the on-resonance version of our code.

Besides showing the excellent agreement between our methods of computing \mathcal{Z}_{lmN}^* , Fig. 2 also illustrates how \mathcal{Z}_{lmN}^* varies with χ_0 . For this example, we find that $|\mathcal{Z}_{lmN}^H|$ varies by about 25% from minimum to maximum, and $|\mathcal{Z}_{lmN}^\infty|$ varies by about 40%. The associated energy fluxes, which are proportional to the amplitude's modulus squared, varies by about 55% and a factor of two, respectively.

Figures 3 and 4 give two examples of the on-resonance rate of change of orbital constants. We show \dot{E}_{lmN}^* and \dot{Q}_{lmN}^* for two orbits about a black hole with $a = 0.9$. Figure 3 shows the $l = 2$, $m = 2$, $N = -5$ mode computed for an orbit with $p = 3.2758M$, $e = 0.7$, $\theta_m = 70^\circ$; in this case, $\Omega_\theta/\Omega_r = 3$. Figure 4 shows the $l = 5$, $m = -2$, $N = 11$ mode for an orbit with $p = 4.5322M$, $e = 0.3$, $\theta_m = 45^\circ$, for which $\Omega_\theta/\Omega_r = 2$.

In both cases, the flux of energy to infinity varies by a factor of about 3.1. This agreement is a coincidence. The down-horizon flux shows more variety, varying by a factor of about 6.8 for the 3:1 resonance, and by a factor of nearly 10^3 for the 2:1 case. (This large variation is because the flux comes close to zero at $\chi_0 \simeq 4.7$.) The variation in $\dot{Q}_{2,2,-5}^\infty$ is especially interesting for the 3:1 resonance: It is negative over nearly half the span of χ_0 , but is positive elsewhere. This behavior is unique to the on-resonance form of \dot{Q}_{lmN}^* , and arises from the fact that it contains a term proportional to $\text{Re}[\mathcal{Z}_{lmN}\bar{\mathcal{Y}}_{lmN}]$. Because the amplitudes \mathcal{Z}_{lmN} and \mathcal{Y}_{lmN} can have different phases, the behavior of \dot{Q}_{lmN}^* can be more complicated

than the behavior of the energy or angular momentum fluxes. Those fluxes are both proportional to $|\mathcal{Z}_{lmN}^*|^2$, and hence are positive or negative definite.

The horizontal dashed lines in these figures gives the rate of change that would be found if the resonance were neglected. In other words, it shows the rate of change one would find by simply combining in quadrature all of the 4-index amplitudes \mathcal{Z}_{lmkn}^* which contribute to the relevant 3-index amplitude $\mathcal{Z}_{lmN}^*(\chi_0)$. Its value is the average with respect to λ_0^θ of the resonant flux:

$$\begin{aligned}\dot{E}_{lmN}^{*, \text{ no-res}} &= \frac{\Upsilon_\theta}{2\pi} \int_0^{2\pi/\Upsilon_\theta} \dot{E}_{lmN}^* d\lambda_0^\theta \\ &= \frac{\Upsilon_\theta}{2\pi} \int_0^{2\pi} \dot{E}_{lmN}^*(\chi_0) \frac{d\lambda_0^\theta}{d\chi_0} d\chi_0.\end{aligned}\quad (4.1)$$

Recall that the parameter λ_0^θ , introduced in Eq. (3.18), sets the value of λ^θ at which $\theta = \theta_m$. An explicit expression for the Jacobian $d\lambda_0^\theta/d\chi_0$ is given in Eq. (3.76) of Ref. [17]. It is not difficult to show that this result must hold³: combining Eqs. (3.34) and (3.35), we have

$$\begin{aligned}\dot{E}_{lmN}^\infty(\chi_0) &= \frac{1}{4\pi\omega_{mN}^2} \left(\sum |\check{\mathcal{Z}}_{lmkn}^H|^2 \right. \\ &\quad \left. + \sum \check{\mathcal{Z}}_{lmkn}^H \bar{\check{\mathcal{Z}}}_{lmk'n'}^H e^{i[\xi_{mkn}(\chi_0) - \xi_{mk'n'}(\chi_0)]} \right).\end{aligned}\quad (4.2)$$

The first sum in this expression is, as usual, taken over all pairs $(k, n)_N$, as defined earlier. The second sum is taken over the pair of pairs $(k, n)_N$ and $(k', n')_N$, with $k \neq k'$, $n \neq n'$. The first sum is exactly $\dot{E}_{lmN}^{\infty, \text{ no-res}}$. Using Eq. (3.18), we see that on resonance,

$$\xi_{mkn} - \xi_{mk'n'} = (k - k')\Upsilon^\theta \lambda_0^\theta.\quad (4.3)$$

Hence this term averages to zero, demonstrating the validity of Eq. (4.1). Similar results hold for all of the other rates of change we compute in this paper.

These examples show that the flux carried in each mode can vary significantly as a function of χ_0 . This shows that in principle resonances can have a strong impact on gravitational-wave fluxes. Notice, though, that the detailed dependence of each mode on χ_0 varies quite a bit from mode to mode. It would not be surprising if much of the variation cancels out after summing over many modes. We examine this in the next section, checking to see how much flux variation remains when many modes are added.

² It is not difficult to do the calculations more accurately than this [29–31], but 6 digits of accuracy is good enough for this first strong-field examination of this effect.

³ At one point in our analysis, preliminary results indicated that averages did not respect Eq. (4.1). Gabriel Perez-Giz insisted to one of us (SAH) that this must be an error. Indeed, these preliminary results were wrong.

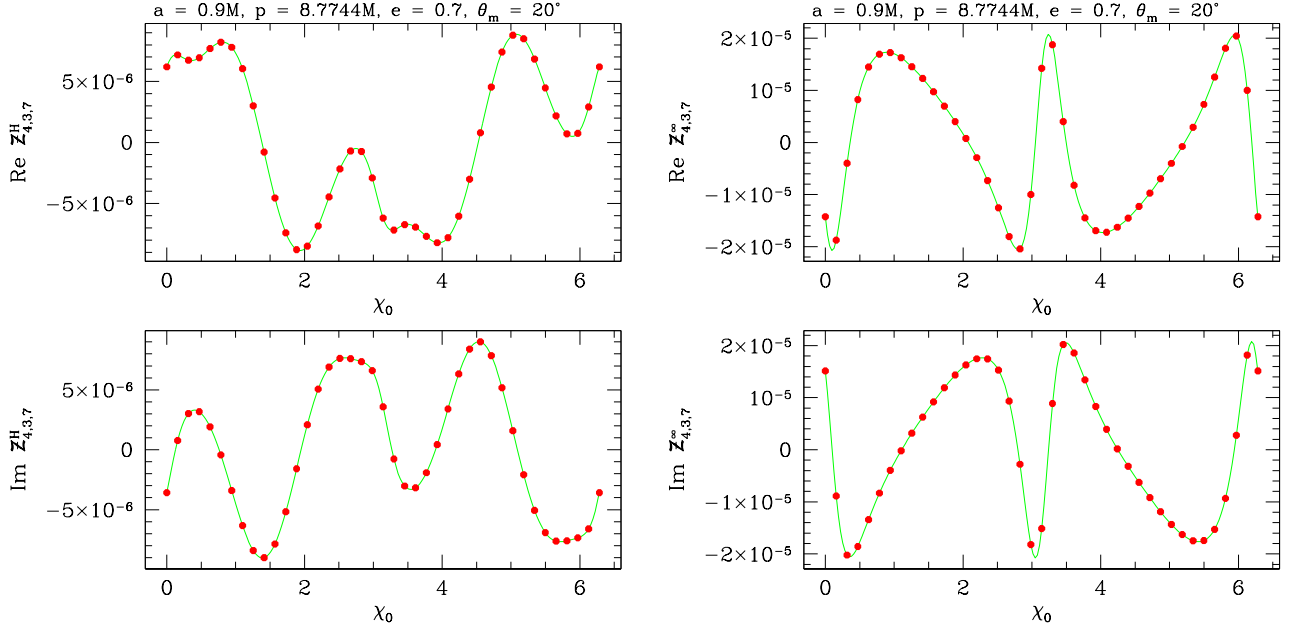


FIG. 2: Comparison of two methods to compute the on-resonance amplitudes Z_{lmN}^* . All panels correspond to radiation from an orbit with parameters $p = 8.7744M$, $e = 0.7$, $\theta_m = 20^\circ$, about a black hole with spin $a = 0.9M$. For this orbit, $\Omega_\theta/\Omega_r = 3/2$. We have chosen $l = 4$, $m = 3$, $N = 7$. Left panels show Z_{437}^H , right panels show Z_{437}^∞ ; top panels show the real part, bottom panels the imaginary part. Green curves show the amplitude computed by the on-resonance merging of amplitudes discussed in Sec. III D; Sec. III E; red dots show the amplitude computed using the constrained source integral presented in Sec. III E. The two methods agree to numerical accuracy (roughly 6 digits in this case).

B. Sum over many modes: Variation of total flux

We now examine the variation in total flux on resonant orbits, computing the sums (3.35) and (3.36). Those sums are taken over an infinite number of modes, which we cannot do in a numerical calculation. We instead truncate the sum over index l at $l_{\max} = 6$; for orbits with $e = 0.3$, we truncate the sum over N at $N_{\max} = 50$, and truncate at $N_{\max} = 100$ for $e = 0.7$:

$$\dot{E}^*(\chi_0) = \sum_{l=2}^{l_{\max}} \sum_{m=-l}^l \sum_{N=-N_{\max}}^{N_{\max}} \dot{E}_{lmN}^*(\chi_0). \quad (4.4)$$

We have not performed a careful convergence analysis, but have found that increasing l_{\max} and N_{\max} only changes our numerical results by an unimportant fraction for the orbits we have examined so far. We do not claim our accuracy to be good enough for “production” purposes, but claim it is good enough to illustrate the physics that we present here.

Figure 5 shows one example of how, after summing over many modes, \dot{E}^* varies as a function of χ_0 . We put $a = 0.9M$, and choose an orbit with $p = 5.48622M$, $e = 0.7$, and $\theta_m = 70^\circ$, for which $\Omega_\theta/\Omega_r = 3/2$. The fractional variation in \dot{E}^* we find is much smaller than the variation we saw in individual modes: the summed flux to infinity varies by about 0.2%, and the down-horizon flux varies by about 6.7%. The down-horizon flux is much smaller than

the flux to infinity, so the variations are dominated by the behavior \dot{E}^∞ . The behaviors of $\dot{L}_z^*(\chi_0)$ and $\dot{Q}^*(\chi_0)$ are qualitatively similar to $\dot{E}^*(\chi_0)$, so we do not show plots for those quantities.

Tables I – IV present the fractional variation in \dot{E}^* , \dot{L}_z^* , and \dot{Q}^* for several orbits about a black hole with spin $a = 0.9M$. Within each table, we fix e and θ_m . We look at large and small eccentricity ($e = 0.7$ and $e = 0.3$), and large and small orbital inclination⁴ ($\theta_m = 20^\circ$ and $\theta_m = 70^\circ$). We then vary p to study radiation emission from four different resonances, 3:1, 2:1, 3:2, and 4:3. The fractional variation in a quantity X is defined as

$$\Delta X \equiv \frac{|X_{\max}| - |X_{\min}|}{(|X_{\max}| + |X_{\min}|)/2}, \quad (4.5)$$

where $X_{\max/\min}$ is the maximum or minimum value X takes as χ_0 varies from 0 to 2π .

The peak-to-trough variation (4.5) in the fluxes is an important quantity that determines several properties of the resonances. First, the “kicks” in E , L_z , and Q that occur as a system spirals through a resonance are directly proportional to the variation (4.5) [32]. Second, there are two qualitatively different types of resonances

⁴ Note that smaller θ_m implies a more highly inclined orbit; $\theta_m = 90^\circ$ is an equatorial orbit.

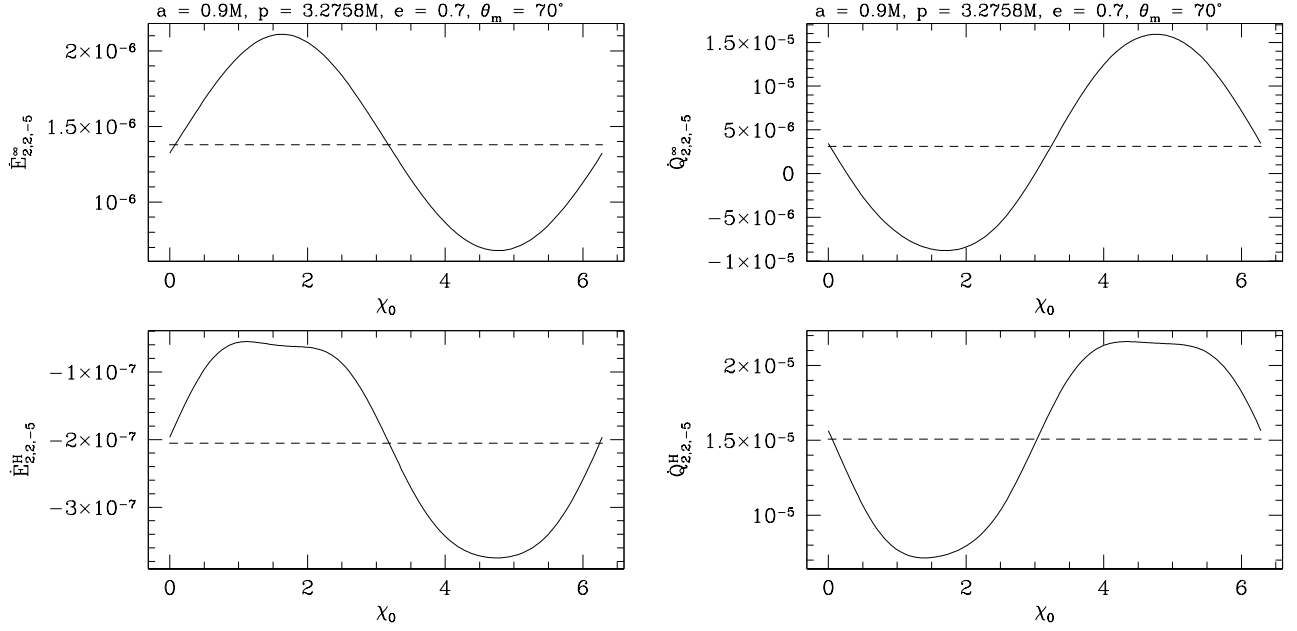


FIG. 3: On-resonance variation of the rates of change of orbital energy (left panels) and Carter constant (right panels) in the $l = 2, m = 2, N = -5$ mode for an orbit with $p = 3.2758M$, $e = 0.7$, $\theta_m = 70^\circ$, $a = 0.9M$ (for which $\Omega_\theta/\Omega_r = 3$). Top panels give the flux to infinity, bottom ones give flux down the horizon. The dashed line in all panels shows the value that would be obtained if the resonance were neglected (i.e., simply adding in quadrature the various 4-index amplitudes Z_{lmkn}^* that contribute to the 3-index amplitude Z_{lmN}^*). In all cases, the flux varies considerably with the phase χ_0 . The variation in \dot{Q}^∞ is especially interesting in this case, changing sign at $\chi_0 \simeq 0.28$ and $\chi_0 \simeq 3.01$. We do not show $\dot{L}_z^*(\chi_0)$ for this mode, since it is identical to $\dot{E}^*(\chi_0)$ modulo a factor of m/ω_{mN} .

that can occur in systems of this kind: a simple linear resonance in which the kicks depend sinusoidally on the phase parameter χ_0 (cf. the final equation of FH), and a nonlinear variant in which the dynamics is rather more complicated. For the nonlinear scenario, it is possible to have a “sustained resonance” in which the system becomes trapped near the resonance for an extended period of time [33, 34]. Our numerical results show that $\Delta X \ll 1$ at least over all of the parameter space we have surveyed so far, which indicates that the resonances are always of the simple, linear kind. This agrees with post-Newtonian analyses [32].

Some interesting trends are apparent from these tables. First, notice that in all cases the down-horizon variation is quite a bit larger than the variation in the quantities to infinity. However, in all cases, the magnitude of the down-horizon fluxes is substantially smaller than the magnitude to infinity. The total variations are thus dominated by the fluxes to infinity, consistent with the results shown in Fig. 5.

Second, notice that the largest variations are seen in either the 2:1 or 3:2 resonances (always the 3:2 resonance for orbits with $e = 0.3$, but either 3:2 or 2:1 depending on which quantity we examine for the orbits with $e = 0.7$). The variations are consistently smallest for the 4:3 resonance. This behavior correlates with the shape that a resonant orbit traces in the (r, θ) plane. Figure 6 shows

these orbital tracks for the four orbits presented in Table I. For simplicity, we only show tracks for $\chi_0 = \pi/2$.

The contrasting shapes of the 2:1 and 3:2 orbits on one hand, and of the 4:3 orbit on the other, are particularly noteworthy. The 4:3 resonant orbit (bottom right) traces a rather complicated Lissajous figure which comes “close to” many of the (r, θ) points which are accessible given (p, e, θ_m) . This complicated trajectory samples much of the accessible domain in r and θ . Appealing to the constrained integral method of computing Z_{lmN}^* (cf. Sec. III E), we can say that the motion effectively averages out the variations in the integrand by passing close to so many accessible points.

By contrast, the trajectory for the 2:1 and 3:2 resonances (top right and bottom left) are much simpler. These trajectories do not come as close to so many points in their allowed domain, and so do not average the variations in their integrands as effectively. The trajectory for the 3:1 (top left) resonance is similar to that for the 2:1 case, but with an additional angular oscillation at small radius. This extra oscillation enhances the averaging as the orbit moves through a particularly strong-field part of its domain. Not too surprisingly, the flux variation in this case is generally intermediate to the others.

Beyond the fact that orbits with simple shapes in the (r, θ) plane tend to show stronger resonances than orbits with more complicated shapes, we do not as yet see

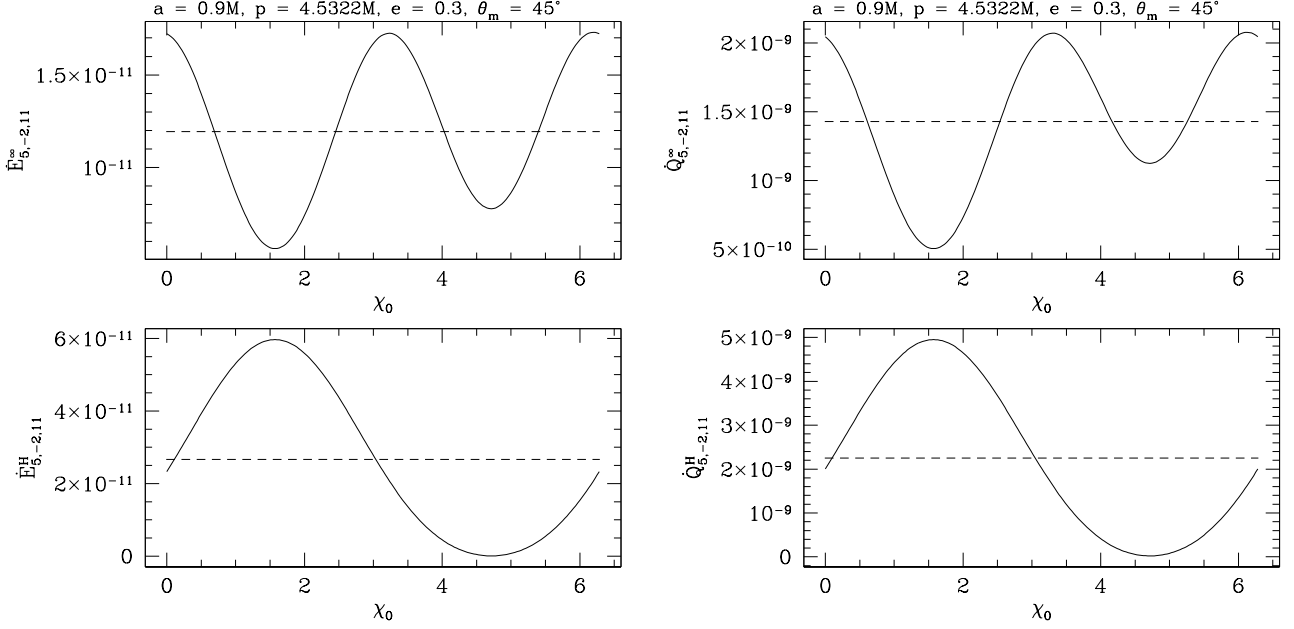


FIG. 4: On-resonance variation of the rates of change of orbital energy (left panels) and Carter constant (right panels) in the $l = 5, m = -2, N = 11$ mode for an orbit with $p = 4.5322M$, $e = 0.3$, $\theta_m = 45^\circ$, $a = 0.9M$ (for which $\Omega_\theta/\Omega_r = 2$). Top panels give the flux to infinity, bottom ones give flux down the horizon. The dashed line gives the value found when the resonance is neglected. As in Fig. 3, we see that \dot{E}_{lmN}^* and \dot{Q}_{lmN}^* vary quite a bit as χ_0 sweeps from 0 to 2π , with minima near zero in this case for the down-horizon quantities.

e	θ_m	p	Ω_θ/Ω_r	$\Delta\dot{E}^H$	$\Delta\dot{L}_z^H$	$\Delta\dot{Q}^H$	$\Delta\dot{E}^\infty$	$\Delta\dot{L}_z^\infty$	$\Delta\dot{Q}^\infty$	$\Delta\dot{E}^{\text{tot}}$	$\Delta\dot{L}_z^{\text{tot}}$	$\Delta\dot{Q}^{\text{tot}}$
0.7	20°	$5.38952M$	3	92.5%	0.363%	0.543%	0.087%	0.069%	0.105%	0.125%	0.027%	0.126%
0.7	20°	$6.31541M$	2	30.7%	2.89%	1.82%	0.634%	0.483%	0.467%	0.662%	0.270%	0.494%
0.7	20°	$8.77436M$	$3/2$	106%	21.9%	10.4%	1.17%	0.172%	0.219%	1.03%	0.489%	0.261%
0.7	20°	$11.4219M$	$4/3$	1.41%	0.117%	0.979%	0.048%	0.058%	0.003%	0.047%	0.060%	0.002%

TABLE I: Variation in flux for orbits with $e = 0.7$ and $\theta_m = 20^\circ$ about a black hole with spin $a = 0.9M$. We vary p to examine a sequence of orbital resonances from $\Omega_\theta/\Omega_r = 3$ to $\Omega_\theta/\Omega_r = 4/3$. Columns 3 – 5 show the fractional variation in energy flux, axial angular momentum flux, and Carter constant rate of change arising from the down-hole fields; the fractional variation is defined precisely in the text. Columns 6 – 8 repeat this information for these fields at infinity, and columns 9 – 11 give the fractional variation for the totals (infinity plus horizon). The variations are largest for the 3:2 resonance and 2:1 resonances (depending on which quantity we examine), and smallest for the 4:3 resonance.

strong evidence of any trend which would allow us to predict which resonances will tend to be “strong” (i.e., exhibit large variation in orbital parameter evolution) and which “weak.” Consider for example the rate of change of orbital energy, $\Delta\dot{E}^{\text{tot}}$. As we go from high inclination to shallow and from high eccentricity to low, we see that $\Delta\dot{E}^{\text{tot}}$ goes from large to small: It takes the value 1.03% for high eccentricity, high inclination (Table I); 0.167% and 0.303% for the mixed cases (Tables II and III); and the value 0.131% for the case of small eccentricity, shallow inclination (Table IV). This appears to suggest, at least roughly, that the strength of the resonance is correlated with the degree of radial and angular motion.

However, no such pattern is seen when we examine $\Delta\dot{L}_z^{\text{tot}}$ and $\Delta\dot{Q}^{\text{tot}}$. For L_z , the high eccentricity, high inclination case again produces the largest variation

(0.489%, in the 3:2 resonance of Table I). However, the *low* eccentricity, *low* inclination case produces the second largest variation (0.123%, in the 3:2 resonance of Table IV). These values of e and θ_m likewise produce the largest and second-largest variations in the Carter constant (albeit in different resonances).

We do not yet have a compelling way to explain these trends (or lack of trends) in the resonances’ strength, so we leave this mystery to future work.

V. CONCLUDING DISCUSSION AND FUTURE WORK

In this analysis, using a Teukolsky-equation-based formalism good for exploring radiation produced by strong-

e	θ_m	p	Ω_θ/Ω_r	$\Delta\dot{E}^H$	$\Delta\dot{L}_z^H$	$\Delta\dot{Q}^H$	$\Delta\dot{E}^\infty$	$\Delta\dot{L}_z^\infty$	$\Delta\dot{Q}^\infty$	$\Delta\dot{E}^{\text{tot}}$	$\Delta\dot{L}_z^{\text{tot}}$	$\Delta\dot{Q}^{\text{tot}}$
0.7	70°	$3.27580M$	3	1.14%	1.89%	2.60%	0.010%	0.067%	0.421%	0.026%	0.009%	0.035%
0.7	70°	$3.78947M$	2	1.60%	2.68%	6.01%	0.204%	0.153%	0.109%	0.167%	0.067%	0.357%
0.7	70°	$5.48622M$	$3/2$	6.66%	5.77%	26.3%	0.222%	0.034%	0.216%	0.127%	0.078%	0.210%
0.7	70°	$7.53814M$	$4/3$	0.042%	0.008%	4.04%	0.001%	0.002%	0.023%	0.001%	0.002%	0.023%

TABLE II: Variation in flux for orbits with $e = 0.7$ and $\theta_m = 70^\circ$ about a black hole with spin $a = 0.9M$. As when $e = 0.7$ and $\theta_m = 70^\circ$, the variations are largest for the 3:2 resonance and 2:1 resonances (depending on which quantity we examine), and smallest for the 4:3 resonance.

e	θ_m	p	Ω_θ/Ω_r	$\Delta\dot{E}^H$	$\Delta\dot{L}_z^H$	$\Delta\dot{Q}^H$	$\Delta\dot{E}^\infty$	$\Delta\dot{L}_z^\infty$	$\Delta\dot{Q}^\infty$	$\Delta\dot{E}^{\text{tot}}$	$\Delta\dot{L}_z^{\text{tot}}$	$\Delta\dot{Q}^{\text{tot}}$
0.3	20°	$5.04884M$	3	4.43%	0.659%	1.15%	0.027%	0.068%	0.054%	0.008%	0.024%	0.033%
0.3	20°	$6.12789M$	2	4.24%	1.42%	1.94%	0.012%	0.025%	0.013%	0.004%	0.080%	0.002%
0.3	20°	$8.65334M$	$3/2$	3.34%	2.62%	8.82%	0.308%	0.158%	0.114%	0.303%	0.123%	0.123%
0.3	20°	$11.3158M$	$4/3$	0.104%	0.165%	1.09%	0.003%	0.005%	0.002%	0.003%	0.004%	0.002%

TABLE III: Variation in flux for orbits with $e = 0.3$ and $\theta_m = 20^\circ$ about a black hole with spin $a = 0.9M$. In this case, the 3:2 resonance shows larger variations than all other cases; the 2:1 resonance is surprisingly weak, given its strength in other examples we have seen. As usual, however, the 4:3 resonance shows the least amount of variation among all the resonances that we consider.

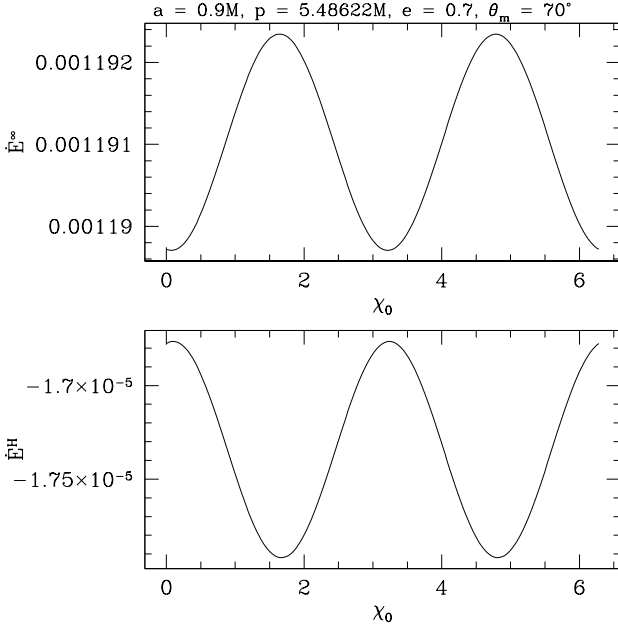


FIG. 5: Variation of total energy flux, both to infinity (top) and down the horizon (bottom) for an orbit with $p = 5.48622M$, $e = 0.7$, $\theta_m = 70^\circ$, $a = 0.9M$ (for which $\Omega_\theta/\Omega_r = 3/2$). After summing over many modes, the variation is significantly reduced: the flux to infinity only varies by about 0.127%, and that down the horizon varies by roughly 1.6%. The variations in $\dot{L}_z(\chi_0)$ and $\dot{Q}^*(\chi_0)$ are qualitatively similar, so we do not show them. See Table II for more details.

field orbits, we have confirmed the picture that on resonance the gravitational-wave driven evolution of a binary can depend strongly on the relative phase of radial and angular motions. A binary in which this relative phase

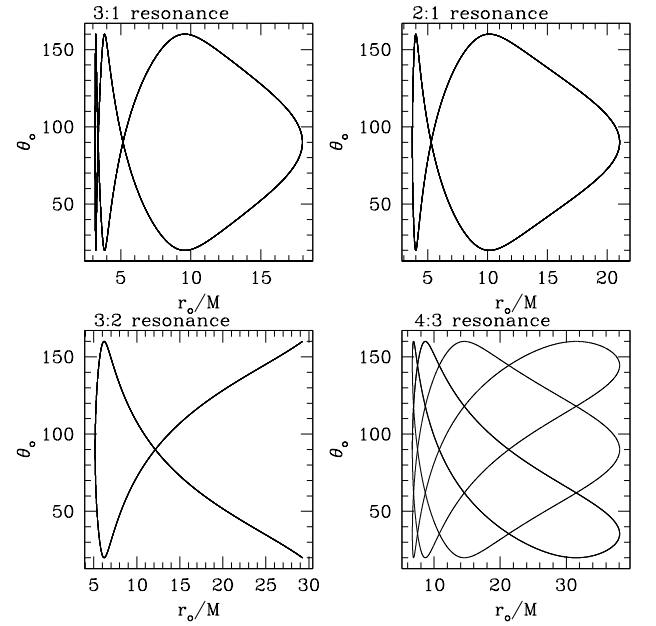


FIG. 6: Trajectories in the (r, θ) plane for the orbits discussed in Table I. We put $\chi_0 = \pi/2$ for these plots. The 4:3 resonance shows the smallest flux variation of those considered here, and has the most complicated trajectory. This orbit comes “close to” enough points in the (r, θ) plane that it averages over much of its accessible domain. By contrast, the 3:2 and 2:1 orbits have simple trajectories and do not effectively average over their domain. Fluxes from these orbits tend to show the largest variation with χ_0 . The 3:1 orbit is similar to the 2:1 orbit, but with an additional angular oscillation at small radius which enhances orbital averaging. This orbit generally shows intermediate flux variation compared with the other cases.

e	θ_m	p	Ω_θ/Ω_r	$\Delta\dot{E}^H$	$\Delta\dot{L}_z^H$	$\Delta\dot{Q}^H$	$\Delta\dot{E}^\infty$	$\Delta\dot{L}_z^\infty$	$\Delta\dot{Q}^\infty$	$\Delta\dot{E}^{\text{tot}}$	$\Delta\dot{L}_z^{\text{tot}}$	$\Delta\dot{Q}^{\text{tot}}$
0.3	70°	2.91117M	3	1.13%	1.17%	0.544%	0.023%	0.026%	0.367%	0.059%	0.070%	0.310%
0.3	70°	3.55601M	2	1.10%	1.28%	3.67%	0.103%	0.142%	0.039%	0.131%	0.179%	0.046%
0.3	70°	5.34138M	3/2	0.481%	0.336%	4.86%	0.106%	0.063%	0.227%	0.102%	0.067%	0.208%
0.3	70°	7.41979M	4/3	0.007%	0.021%	0.229%	0.001%	0.001%	0.006%	0.001%	0.001%	0.006%

TABLE IV: Variation in flux for orbits with $e = 0.3$ and $\theta_m = 70^\circ$ about a black hole with spin $a = 0.9M$. The case is qualitatively similar to most of the others, with the 3:2 and 2:1 showing the largest degree of variation (depending on the quantity being examined), and the 4:3 case showing the least.

has the value $\pi/2$ as the system enters resonance may evolve quite differently from an otherwise identical system in which this phase is $3\pi/2$ entering resonance. A typical extreme mass ratio binary can be expected to pass through several orbital resonances en route to its final coalescence. That their evolution through each resonance depends strongly on an “accidental” phase parameter has the potential to complicate schemes for measuring gravitational waves from these binaries.

We find that the degree of variation depends strongly upon the topology of the orbital trajectory in the (r, θ) plane. Of the cases we have studied in detail, the orbital plane trajectory of resonances like $\Omega_\theta/\Omega_r = 3/2$ have a simple topology. This trajectory does not cross itself very often, and does not come close to many points in the plane. Such resonances do not effectively average out the behavior of the source to the wave equation. As such, if the source varies significantly over an orbit, there can be a strong residue of this variation in the associated radiation. By contrast, the trajectory of resonances like $\Omega_\theta/\Omega_r = 4/3$ has a more complicated topology, crossing itself many times, and more completely “covering” the plane. In these cases, the orbit comes “close to” many of the allowed points in the (r, θ) plane, which quite effectively averages out the source’s behavior.

Although instructive and a nice validation of our ability to examine resonances, these results are not enough to truly assess the importance that resonances have in a strong field analysis. We must be able to analyze a system as it evolves through a resonance, and thereby integrate the full “kicks” in the integrals of motion E , L_z , and Q imparted to the system as it passes through resonance. To do this, we have begun expanding our Teukolsky code to compute, in the frequency domain, the instantaneous components of the dissipative or radiative piece of the self-force. Our formulation is based on the discussion in Refs. [12, 13], and is similar to the prescription described in Ref. [17] for scalar self forces⁵. This will allow us to study how a real inspiral is affected as

we evolve through each resonance using results that are good deep in the strong field. The results shown in this paper are a first step toward this, demonstrating that our strong-field toolkit can be used to study resonant effects.

Acknowledgments

The code used in this analysis was derived from that first presented in Ref. [19]; we thank Steve Drasco for his contributions to that work and the development of this code. We thank Tanja Hinderer, Amos Ori, Nicolás Yunes, and Janna Levin for useful discussions in the course of this research. We particularly thank Gabriel Perez-Giz, whose discussion of how the on-resonant fluxes should average away was helpful in tracking down a bug as we were developing this paper. Our work was supported at MIT by NSF grant PHY-1068720 and by NASA Grant NNX08AL42G, and at Cornell by NSF grant PHY-1068541. SAH also gratefully acknowledges fellowship support by the John Simon Guggenheim Memorial Foundation, and sabbatical support from the Canadian Institute for Theoretical Astrophysics and the Perimeter Institute for Theoretical Physics. UR gratefully acknowledges fellowship support from the Royal Thai Government.

Appendix A: Proof: Equivalence of methods for computing on-resonant amplitudes

In this appendix, we prove that Eq. (3.45), the 1-D integral for the on-resonance 3-index amplitude $Z_{lmN}^*(\chi_0)$, is equivalent to Eq. (3.34), the on-resonance amplitude expressed as a sum of 4-index amplitudes $Z_{lmkn}^*(\chi_0)$, each of which is computed using the 2-D integral (3.14).

We begin with Eq. (3.6), which we repeat here:

$$Z_{lm\omega}^*(\chi_0) = C^* \int_{-\infty}^{\infty} d\lambda e^{i(\omega\Gamma - m\Upsilon_\phi)\lambda} J_{lm\omega}^*[r_o(\lambda), \theta_o(\lambda, \chi_0)] . \quad (\text{A1})$$

Recall that the “o” subscript on r and θ means that those are quantities along the orbit, and as such vary at harmonics of the frequencies Υ_r and Υ_θ . We can thus ex-

⁵ One might be concerned about gauge ambiguities associated with the gravitational self force. As shown by Mino [11], these ambiguities disappear when one averages the self force’s effects over an infinite time. In a two-timescale expansion [10], such ambiguities remain, but are suppressed by the ratio of the timescales.

pand $J_{lm\omega}^*$ in a Fourier series:

$$J_{lm\omega}^* = \sum_{kn} J_{\omega l m k n}^*(\chi_0) e^{-i(k\Upsilon_\theta + n\Upsilon_r)\lambda}, \quad (\text{A2})$$

$$= \sum_N \mathcal{J}_{\omega l m N}^*(\chi_0) e^{-iN\Upsilon\lambda}. \quad (\text{A3})$$

Equation (A2) holds for arbitrary orbits. Equation (A3) only holds on resonance, when $\Upsilon_\theta = \beta_\theta \Upsilon$, $\Upsilon_r = \beta_r \Upsilon$.

Because Eq. (A2) remains valid for resonant orbits, in the resonant case

$$\sum_N \mathcal{J}_{\omega l m N}^*(\chi_0) e^{-iN\Upsilon\lambda} \doteq \sum_{kn} J_{\omega l m k n}^*(\chi_0) e^{-i(k\Upsilon_\theta + n\Upsilon_r)\lambda}. \quad (\text{A4})$$

(The notation “ \doteq ” means that this equation is true only on resonance.) Multiply both sides by $e^{iN'\Upsilon\lambda}$ and integrate from 0 to $2\pi/\Upsilon$. On the left-hand side, we have

$$\begin{aligned} \int_0^{2\pi/\Upsilon} \sum_N \mathcal{J}_{\omega l m N}^*(\chi_0) e^{i(N'-N)\Upsilon\lambda} d\lambda \\ = \frac{2\pi}{\Upsilon} \sum_N \mathcal{J}_{\omega l m N}^*(\chi_0) \delta_{N N'} \\ = \frac{2\pi}{\Upsilon} \mathcal{J}_{\omega l m N'}^*(\chi_0). \end{aligned} \quad (\text{A5})$$

To do this operation on the right-hand side, first note that by the resonance condition we must have

$$k\Upsilon_\theta + n\Upsilon_r = (k\beta_\theta + n\beta_r)\Upsilon. \quad (\text{A6})$$

Using this, the integral for the right-hand side becomes

$$\begin{aligned} \int_0^{2\pi/\Upsilon} \sum_{kn} J_{\omega l m k n}^*(\chi_0) e^{i[N' - (k\beta_\theta + n\beta_r)]\Upsilon\lambda} d\lambda \\ = \frac{2\pi}{\Upsilon} \sum_{kn} J_{\omega l m k n}^*(\chi_0) \delta_{(k\beta_\theta + n\beta_r), N'} \\ = \frac{2\pi}{\Upsilon} \sum_{(k,n)_{N'}} J_{\omega l m k n}^*(\chi_0). \end{aligned} \quad (\text{A7})$$

The notation $(k, n)_{N'}$ means that the sum is over all pairs (k, n) which satisfy $k\beta_\theta + n\beta_r = N'$.

Next, use Eqs. (3.13), (3.15) and (3.44), invoke Eq. (3.34), drop the primes on the index N , and equate (A5) and (A7). The result is

$$\mathcal{Z}_{lmN}^*(\chi_0) \doteq \sum_{(k,n)_N} e^{i\xi_{mkn}(\chi_0)} \check{Z}_{lmkn}^*, \quad (\text{A8})$$

which proves that the 1-D integral and the sum of 2-D integrals are equivalent for resonant orbits.

Appendix B: Evolution of the Carter constant

The third conserved quantity associated with orbits of Kerr black holes is the Carter constant, Q . Rearranging Eq. (2.2), we write

$$Q = \cot^2 \theta L_z^2 + \cos^2 \theta (1 - E^2) + \left(\frac{d\theta}{d\lambda} \right)^2. \quad (\text{B1})$$

Reference [21] (S06) first demonstrated how to compute the long-time-averaged evolution of Q , at least for non-resonant orbits. In this appendix, we revisit their calculation in some detail in order to see clearly how it will have to be modified for resonant orbits (modifying some details to be in accord with our notation). We then examine how the calculation changes when we are on an orbital resonance.

1. Setup

We begin with the first line of Eq. (3.18) of S06. It relates the averaged rate of change of the Carter constant, per unit Mino time, to the Kerr metric's Killing tensor $K^{\alpha\beta}$ and to a radiative field Ψ_{rad} which is constructed from the perturbation to the Kerr spacetime metric:

$$\left\langle \frac{dK}{d\lambda} \right\rangle \equiv \lim_{L \rightarrow \infty} \frac{1}{2L} \int_{-L}^L d\lambda \frac{dK}{d\lambda} = \lim_{L \rightarrow \infty} \frac{1}{2L} \int_{-L}^L d\lambda \left[2\Sigma K^{\alpha\beta} \tilde{u}_\alpha \partial_\beta \left(\frac{\Psi_{\text{rad}}}{\Sigma} \right) \right] \Big|_{x \rightarrow z(\lambda)}. \quad (\text{B2})$$

We refer the reader to S06 for a detailed derivation of Eq. (B2), and defer discussion of the radiative field $\Psi_{\text{rad}}(x)$ to Secs. B3 and B4. The coordinate x represents a general spacetime field point; $x \rightarrow z(\lambda)$ means to take this general point to the orbit's worldline $z(\lambda)$.

The other quantities appearing in Eq. (B2) are as follows: First, K is a variant of the Carter constant, given by

$$K = Q + (L_z - aE)^2. \quad (\text{B3})$$

It is related to the Kerr metric's Killing tensor by

$$K = K^{\alpha\beta} u_\alpha u_\beta , \quad (\text{B4})$$

where

$$K^{\alpha\beta} = 2\Sigma m^{(\alpha} \bar{m}^{\beta)} - a^2 \cos^2 \theta g^{\alpha\beta} . \quad (\text{B5})$$

The tensor $g^{\alpha\beta}$ is the Kerr metric, and m^α are components of the Newman-Penrose tetrad leg,

$$m^t = \frac{ia \sin \theta}{\sqrt{2}(r + ia \cos \theta)} , \quad m^r = 0 , \quad m^\theta = \frac{1}{\sqrt{2}(r + ia \cos \theta)} , \quad m^\phi = \frac{i \csc \theta}{\sqrt{2}(r + ia \cos \theta)} . \quad (\text{B6})$$

Overbar denotes complex conjugate. The quantity \tilde{u}_α is the 4-velocity promoted to a spacetime field:

$$(\tilde{u}_t, \tilde{u}_r, \tilde{u}_\theta, \tilde{u}_\phi) = (-E, \pm \sqrt{R(r)}/\Delta, \pm \sqrt{\Theta(\theta)}, L_z) , \quad (\text{B7})$$

where $R(r)$ is defined in Eq. (2.1), and $\Theta(\theta)$ in Eq. (2.2). Notice that our \tilde{u}_θ differs from that used in S06. This is due to a difference in the definition of the potential Θ (it describes motion in θ here, but motion in $\cos \theta$ in S06). The field \tilde{u}_α reduces exactly to the 4-velocity u_α when we take the limit of the field point x to the worldline $z(\lambda)$.

2. General simplification

We now take the first steps in simplifying Eq. (B2). These steps are the same for both resonant and non-resonant cases; we specialize to those cases in Secs. B3 and B4.

We begin by focusing on the integrand of Eq. (B2):

$$\left[2\Sigma K^{\alpha\beta} \tilde{u}_\alpha \partial_\beta \left(\frac{\Psi_{\text{rad}}}{\Sigma} \right) \right] \Big|_{x \rightarrow z(\lambda)} = \left[4\Sigma^2 m^{(\alpha} \bar{m}^{\beta)} \tilde{u}_\alpha \partial_\beta \left(\frac{\Psi_{\text{rad}}}{\Sigma} \right) - 2\Sigma a^2 \cos^2 \theta \tilde{u}^\alpha \partial_\alpha \left(\frac{\Psi_{\text{rad}}}{\Sigma} \right) \right] \Big|_{x \rightarrow z(\lambda)} . \quad (\text{B8})$$

Use the fact that $\tilde{u}^\alpha = u^\alpha$ in the limit $x \rightarrow z(\lambda)$, and that $\Sigma u^\alpha = dx^\alpha/d\lambda$. Expanding $m^{(\alpha} \bar{m}^{\beta)}$, we find

$$2\Sigma K^{\alpha\beta} \tilde{u}_\alpha \partial_\beta \left(\frac{\Psi_{\text{rad}}}{\Sigma} \right) = 2\Sigma \left[(L_z - a \sin^2 \theta E) (\csc^2 \theta \partial_\phi + a \partial_t) + \frac{d\theta}{d\lambda} \partial_\theta \right] \left(\frac{\Psi_{\text{rad}}}{\Sigma} \right) - 2a^2 \cos^2 \theta \frac{d}{d\lambda} \left(\frac{\Psi_{\text{rad}}}{\Sigma} \right) . \quad (\text{B9})$$

[For brevity, we omit $x \rightarrow z(\lambda)$ in Eqs. (B9) and (B10), though it should be understood that this limit is taken.] The right-hand side of Eq. (B9) can be simplified significantly by combining the term in $d\theta/d\lambda$ with the final term:

$$\begin{aligned} 2\Sigma \frac{d\theta}{d\lambda} \partial_\theta \left(\frac{\Psi_{\text{rad}}}{\Sigma} \right) - 2a^2 \cos^2 \theta \frac{d}{d\lambda} \left(\frac{\Psi_{\text{rad}}}{\Sigma} \right) &= 2 \frac{d\theta}{d\lambda} \partial_\theta \Psi_{\text{rad}} - 2 \frac{\Psi_{\text{rad}}}{\Sigma} \frac{d\theta}{d\lambda} \partial_\theta \Sigma \\ &\quad - 2a^2 \frac{d}{d\lambda} \left(\cos^2 \theta \frac{\Psi_{\text{rad}}}{\Sigma} \right) + 2a^2 \frac{\Psi_{\text{rad}}}{\Sigma} \frac{d}{d\lambda} (\cos^2 \theta) . \end{aligned} \quad (\text{B10})$$

The third term on the right-hand side of Eq. (B10) is a total derivative in $d/d\lambda$. Thanks to the periodic nature of all the relevant terms, it will not contribute to an averaging integral of the form (B2), and may be discarded. Using

$$\partial_\theta \Sigma = a^2 \partial_\theta \cos^2 \theta , \quad \frac{d}{d\lambda} \cos^2 \theta = \frac{d\theta}{d\lambda} \partial_\theta \cos^2 \theta , \quad (\text{B11})$$

we see that the second and fourth terms on the right-hand side of (B10) cancel; only the term in $\partial_\theta \Psi_{\text{rad}}$ remains. The integrand simplifies to

$$\left[2\Sigma K^{\alpha\beta} \tilde{u}_\alpha \partial_\beta \left(\frac{\Psi_{\text{rad}}}{\Sigma} \right) \right] \Big|_{x \rightarrow z(\lambda)} = \left\{ 2 \left[(L_z - a \sin^2 \theta E) (\csc^2 \theta \partial_\phi + a \partial_t) + \frac{d\theta}{d\lambda} \partial_\theta \right] \Psi_{\text{rad}} \right\} \Big|_{x \rightarrow z(\lambda)} . \quad (\text{B12})$$

The radiative field Ψ_{rad} can be broken into an “out” and a “down” component:

$$\Psi_{\text{rad}} = \Psi_{\text{rad}}^{\text{out}} + \Psi_{\text{rad}}^{\text{down}} . \quad (\text{B13})$$

These two fields are in turn computed from mode functions $\Phi_{lm\omega}$ (discussed in more detail momentarily) as follows:

$$\Psi_{\text{rad}}^{\text{out}}(x) = \int d\omega \sum_{lm} \frac{1}{4i\omega^3} \left[\Phi_{lm\omega}^{\text{out}}(x) \int d\lambda' \bar{\Phi}_{lm\omega}^{\text{out}}[z(\lambda')] \right] + \text{c.c.}, \quad (\text{B14})$$

$$\Psi_{\text{rad}}^{\text{down}} = \int d\omega \sum_{lm} \frac{1}{4i\omega^2 p_m} \left[\Phi_{lm\omega}^{\text{down}}(x) \int d\lambda' \bar{\Phi}_{lm\omega}^{\text{down}}[z(\lambda')] \right] + \text{c.c.} \quad (\text{B15})$$

In Eq. (B15), $p_m = \omega - m\Omega_H$, where $\Omega_H = a/2Mr_+$ is the angular velocity associated with the event horizon. The abbreviation “c.c.” means complex conjugate. See S06 for further discussion and derivation of these forms of the fields $\Psi_{\text{rad}}^{\text{out}}$ and $\Psi_{\text{rad}}^{\text{down}}$. We will largely focus on the “out” field, which is related to radiation at \mathcal{I}^+ . Extension to the “down” field, related to radiation on the event horizon, is straightforward.

To proceed, we use two equivalent forms for $\Phi_{lm\omega}^{\text{out}}(x)$ evaluated in the limit $x \rightarrow z(\lambda)$; both are described in more detail in S06. The first is up to a constant factor the complex conjugate of the integrand in the expression (3.6) for $Z_{lm\omega}^H$:

$$\Phi_{lm\omega}^{\text{out}}[z(\lambda)] = \bar{J}_{lm\omega}^H(\lambda) e^{-i\lambda(\Gamma\omega - m\Upsilon_\phi)}. \quad (\text{B16})$$

Here Γ is the factor introduced in Sec. II B that converts the mean accumulation of Mino time to the mean accumulation of coordinate time. Equation (B16) is Eq. (3.11) of S06, translated into our notation⁶; the scalar-case version of this equation is Eq. (9.20) of Ref. [17]. Using the Fourier series expansion (3.10) of $J_{lm\omega}^H$, integrating with respect to λ , and combining with the definitions (3.13) and (3.15) gives

$$\int d\lambda' \bar{\Phi}_{lm\omega}^{\text{out}}[z(\lambda')] = \sum_{nk} Z_{lmkn}^H \delta(\omega - \omega_{mkn}), \quad (\text{B17})$$

and so

$$\Psi_{\text{rad}}^{\text{out}}(x) = \int d\omega \left[\sum_{lmkn} \frac{Z_{lmkn}^H \delta(\omega - \omega_{mkn})}{4i\omega^3} \Phi_{lm\omega}^{\text{out}}(x) \right] + \text{c.c.} \quad (\text{B18})$$

A similar simplification describes $\Psi_{\text{rad}}^{\text{down}}(x)$. Combining this with Eqs. (B2) and (B12), we obtain

$$\left\langle \frac{dK^\infty}{d\lambda} \right\rangle = \left\langle \sum_{lmkn} \frac{Z_{lmkn}^H}{2i\omega_{mkn}^3} \left\{ \left[(\csc^2 \theta L_z - aE) \partial_\phi + a(L_z - aE \sin^2 \theta) \partial_t + \frac{d\theta}{d\lambda} \partial_\theta \right] \Phi_{lmkn}^{\text{out}} \right\} + \text{c.c.} \right\rangle, \quad (\text{B19})$$

where $\Phi_{lmkn}^{\text{out}} \equiv \Phi_{lm\omega_{mkn}}^{\text{out}}$. (The superscript “ ∞ ” is because we focus on the “out” field.)

We next manipulate the term in ∂_θ in Eq. (B19), by invoking the second form for $\Phi_{lm\omega}^{\text{out}}(x)$, which is

$$\Phi_{lmkn}^{\text{out}}(x) = f_{lmkn}(r, \theta) e^{im\phi} e^{-i\omega_{mkn}t}. \quad (\text{B20})$$

The value of $f_{lmkn}(r, \theta)$ is not important for our purposes; see S06 [Eq. (3.20) and nearby text] for further details. We have changed notation from S06 slightly to highlight the fact that this function depends on l , m , k , and n ; this is important for generalizing to resonant orbits. We now evaluate on the worldline $x \rightarrow z(\lambda)$, and use the following explicit representations of the motions in t and ϕ :

$$\begin{aligned} t(\lambda) &= \Gamma\lambda + \Delta t_r(\lambda) + \Delta t_\phi(\lambda), \\ \phi(\lambda) &= \Upsilon_\phi\lambda + \Delta\phi_r(\lambda) + \Delta\phi_\phi(\lambda), \end{aligned} \quad (\text{B21})$$

cf. Eqs. (3.8) and (3.9) above and Sec. 3 of Ref. [17]. Here the function Δt_r is periodic with period Λ_r and Δt_θ is periodic with period Λ_θ , etc. This gives

$$\Phi_{lmkn}^{\text{out}}(\lambda) = f_{lmkn}[r(\lambda), \theta(\lambda)] \exp \{ -i\lambda(k\Upsilon_\theta + n\Upsilon_r) - i\omega_{mkn}[\Delta t_r(\lambda) + \Delta t_\theta(\lambda)] + im[\Delta\phi_r(\lambda) + \Delta\phi_\theta(\lambda)] \}. \quad (\text{B22})$$

⁶ Note that there are two errors in Eq. (3.11) of S06: the sign of the exponential is flipped, and the coefficients Z are of the usual type (3.15) rather than the required more general type (3.14) with $\omega \neq \omega_{mkn}$. See Eq. (B30) below.

We next define a mode function of two variables $(\lambda^r, \lambda^\theta)$ by

$$\Phi_{lmkn}^{\text{out}}(\lambda^r, \lambda^\theta) = f_{lmkn}[r(\lambda^r), \theta(\lambda^\theta)] \exp \left\{ -ik\Upsilon_\theta \lambda^\theta - in\Upsilon_r \lambda^r - i\omega_{mkn}[\Delta t_r(\lambda^r) + \Delta t_\theta(\lambda^\theta)] + im[\Delta \phi_r(\lambda^r) + \Delta \phi_\theta(\lambda^\theta)] \right\}. \quad (\text{B23})$$

This function is determined uniquely by the following three properties: First, it reduces to the expression (B22) when evaluated at $\lambda^r = \lambda^\theta = \lambda$; second, it is biperiodic, with a period of Λ^r in λ^r , and of Λ^θ in λ^θ ; and third, it is a continuous function of the geodesic's parameters. The first two properties are sufficient to guarantee uniqueness for non-resonant orbits, but not for resonant orbits since the different periodicities become degenerate. Adding the third property is sufficient to restore uniqueness for all orbits, since resonant orbits form a set of measure zero in the phase space. See Refs. [17, 24] for more details on the mapping between functions of λ and functions of $(\lambda^r, \lambda^\theta)$.

Next, differentiating the explicit expression (B23) with respect to λ^θ , we obtain the following identity relating the differential operator $d/d\lambda^\theta$ and the partial derivative operators ∂_θ , ∂_t and ∂_ϕ acting on Φ_{lmkn}^{out} :

$$\frac{d\theta}{d\lambda} \partial_\theta = \frac{d}{d\lambda^\theta} + ik\Upsilon_\theta - \frac{d\Delta t_\theta}{d\lambda^\theta} \partial_t - \frac{d\Delta \phi_\theta}{d\lambda^\theta} \partial_\phi. \quad (\text{B24})$$

We now use the identity (B24) to substitute for the $(d\theta/d\lambda)\partial_\theta$ term in Eq. (B19). This yields

$$\begin{aligned} \left\langle \frac{dK^\infty}{d\lambda} \right\rangle &= \left\langle \sum_{lmkn} \frac{Z_{lmkn}^H}{2i\omega_{mkn}^3} \right. \\ &\quad \times \left[\left(\csc^2 \theta L_z - aE - \frac{d\Delta \phi_\theta}{d\lambda^\theta} \right) \partial_\phi + \left(aL_z - a^2 E \sin^2 \theta - \frac{d\Delta t_\theta}{d\lambda^\theta} \right) \partial_t + ik\Upsilon_\theta + \frac{d}{d\lambda^\theta} \right] \Phi_{lmkn}^{\text{out}} \left. \right\rangle + \text{c.c.} \end{aligned} \quad (\text{B25})$$

Using Eqs. (3.43) and (3.58) of Ref. [17] it is not difficult to show that

$$\csc^2 \theta L_z - aE - \frac{d\Delta \phi_\theta}{d\lambda^\theta} = \langle \csc^2 \theta L_z - aE \rangle = \langle \csc^2 \theta \rangle L_z - aE, \quad (\text{B26})$$

$$aL_z - a^2 E \sin^2 \theta - \frac{d\Delta t_\theta}{d\lambda^\theta} = \langle aL_z - a^2 E \sin^2 \theta \rangle = aL_z - a^2 E \langle \sin^2 \theta \rangle. \quad (\text{B27})$$

Combining this with Eq. (B25) and using the replacements $\partial_\phi \rightarrow im$, $\partial_t \rightarrow -i\omega_{mkn}$ gives

$$\left\langle \frac{dK^\infty}{d\lambda} \right\rangle = \left\langle \sum_{lmkn} \frac{Z_{lmkn}^H}{2i\omega_{mkn}^3} \left\{ \left[i\mathcal{M}_{mkn} + ik\Upsilon_\theta + \frac{d}{d\lambda^\theta} \right] \Phi_{lmkn}^{\text{out}} \right\} + \text{c.c.} \right\rangle, \quad (\text{B28})$$

where we have defined

$$\mathcal{M}_{mkn} = m(\langle \csc^2 \theta \rangle L_z - aE) - a\omega_{mkn}(L_z - aE \langle \sin^2 \theta \rangle). \quad (\text{B29})$$

Next, from Eqs. (B16), (3.10), (3.13) and (3.15) we obtain an expression for $\Phi_{lmkn}^{\text{out}}(\lambda)$. Extending this to a function of $\lambda^r, \lambda^\theta$ as above gives

$$\Phi_{lmkn}^{\text{out}}(\lambda^r, \lambda^\theta) = \frac{\Gamma}{2\pi} \sum_{\Delta n, \Delta k} \bar{Z}_{\omega_{mkn}lmk+\Delta k, n+\Delta n}^H e^{i\Delta k \Upsilon_\theta \lambda^\theta} e^{i\Delta n \Upsilon_r \lambda^r}. \quad (\text{B30})$$

Combining this with Eq. (B28) yields the final result

$$\left\langle \frac{dK^\infty}{d\lambda} \right\rangle = \left\langle \frac{\Gamma}{4\pi} \sum_{lmkn} \sum_{\Delta k, \Delta n} [\mathcal{M}_{mkn} + k\Upsilon_\theta + \Delta k \Upsilon_\theta] \frac{Z_{lmkn}^H}{\omega_{mkn}^3} \bar{Z}_{\omega_{mkn}lmk+\Delta k, n+\Delta n}^H e^{i\Delta k \Upsilon_\theta \lambda^\theta} e^{i\Delta n \Upsilon_r \lambda^r} + \text{c.c.} \right\rangle. \quad (\text{B31})$$

Here it is understood that the averaging procedure is to first evaluate at $\lambda^r = \lambda^\theta \equiv \lambda$ and then average over λ . In Sec. B3, we evaluate this average for non-resonant orbits, and reproduce the results of S06. In Sec. B4, we do so for a resonant orbit and find an appropriately modified variant of their formula.

3. Non-resonant result

We evaluate the expression (B31) at $\lambda^r = \lambda^\theta \equiv \lambda$ and then evaluate the average over λ defined by Eq. (B2). The term labeled by $\Delta n, \Delta k$ is proportional to

$$\lim_{L \rightarrow \infty} \frac{1}{2L} \int_{-L}^L d\lambda e^{i\Delta k \Upsilon_\theta \lambda} e^{i\Delta n \Upsilon_r \lambda} = \lim_{L \rightarrow \infty} \text{Si}[(\Delta k \Upsilon_\theta + \Delta n \Upsilon_r)L], \quad (\text{B32})$$

where $\text{Si}(x) = \sin(x)/x$. Since the frequencies Υ_θ and Υ_r are incommensurate for non-resonant orbits, the combination $\Delta k \Upsilon_\theta + \Delta n \Upsilon_r$ will be nonvanishing for $(\Delta k, \Delta n) \neq (0, 0)$, and the right hand side will vanish. Thus the only non-vanishing term will be the term with $\Delta n = \Delta k = 0$. Another way to think about this is that we are averaging over a curve which is ergodically filling up the torus parameterized by λ^r and λ^θ , and so the curve average can be replaced by an average over the torus,

$$\lim_{L \rightarrow \infty} \frac{1}{2L} \int_{-L}^L \dots d\lambda \rightarrow \frac{\Upsilon_\theta \Upsilon_r}{(2\pi)^2} \int_0^{2\pi/\Upsilon_\theta} \int_0^{2\pi/\Upsilon_r} \dots d\lambda^r d\lambda^\theta. \quad (\text{B33})$$

Applying this torus average to the expression (B31) again forces $\Delta n = \Delta k = 0$. Now using the definition (3.15) we obtain the final result

$$\left\langle \frac{dK^\infty}{d\lambda} \right\rangle = \Gamma \sum_{lmkn} \frac{|\tilde{Z}_{lmkn}^H|^2}{4\pi\omega_{mkn}^3} [\mathcal{M}_{mkn} + k\Upsilon_\theta] + \text{c.c.} \quad (\text{B34})$$

Because all the terms on the right-hand side of (B34) are real, the complex conjugate simplifies to an overall factor of two. We take the long-time average, so

$$\left\langle \frac{dK}{d\lambda} \right\rangle = \Gamma \left\langle \frac{dK}{dt} \right\rangle. \quad (\text{B35})$$

Further, by Eq. (B3),

$$\frac{dK}{dt} = \frac{dQ}{dt} + 2(aE - L_z) \left(a \frac{dE}{dt} - \frac{dL_z}{dt} \right). \quad (\text{B36})$$

Combining Eqs. (3.25), (3.26), (3.31), (B29) together with Eqs. (B34), (B35), and (B36), we finally obtain

$$\begin{aligned} \left\langle \frac{dQ^\infty}{dt} \right\rangle &= \sum_{lmkn} \frac{|\tilde{Z}_{lmkn}^H|^2}{2\pi\omega_{mkn}^3} (m\langle \cot^2 \theta \rangle L_z - a^2 \omega_{mkn} \langle \cos^2 \theta \rangle E + k\Upsilon_\theta) \\ &\equiv 2 \sum_{lmkn} \frac{\dot{E}_{lmkn}^\infty}{\omega_{mkn}} \mathcal{L}_{mkn}. \end{aligned} \quad (\text{B37})$$

A similar calculation focusing on the “down” modes yields

$$\begin{aligned} \left\langle \frac{dQ^H}{dt} \right\rangle &= \sum_{lmkn} \frac{\alpha_{lmkn} |\tilde{Z}_{lmkn}^\infty|^2}{2\pi\omega_{mkn}^3} (m\langle \cot^2 \theta \rangle L_z - a^2 \omega_{mkn} \langle \cos^2 \theta \rangle E + k\Upsilon_\theta) \\ &= 2 \sum_{lmkn} \frac{\dot{E}_{lmkn}^H}{\omega_{mkn}} \mathcal{L}_{mkn}. \end{aligned} \quad (\text{B38})$$

The factor α_{lmkn} is introduced in Sec. III B; on the second line, we have used Eqs. (3.27) and (3.31). Equations (B37) and (B38) are the same (modulo minor changes in notation) as Eq. (3.26) of S06.

4. Resonant \dot{Q}

We now return to the general formula (B31) evaluated at $\lambda^r = \lambda^\theta = \lambda$ and compute the average over λ for the case of resonant orbits. Before evaluating this average we first simplify the sums over Δk and Δn by rewriting them in terms of $k' = k + \Delta k$, $n' = n + \Delta n$. We also make the replacements

$$\sum_{kn} \rightarrow \sum_N \sum_{(k,n)_N}, \quad \sum_{k'n'} \rightarrow \sum_{N'} \sum_{(k',n')_{N'}}, \quad (\text{B39})$$

where the indicated sums are taken over k, n satisfying $k\beta_\theta + n\beta_r = N$ and over k', n' satisfying $k'\beta_\theta + n'\beta_r = N'$. We note that the quantities \mathcal{M}_{mkn} and ω_{mkn} depend on k and n only through N , and write these as \mathcal{M}_{mN} and ω_{mN} . Finally using the definition (3.34) of the amplitudes \mathcal{Z}_{lmN}^* , the expression (B31) reduces to

$$\left\langle \frac{dK^\infty}{d\lambda} \right\rangle = \left\langle \frac{\Gamma}{4\pi} \sum_{lmN} \sum_{N'} \sum_{(k', n')_{N'}} [\mathcal{M}_{mN} + k'\Upsilon_\theta] \frac{\mathcal{Z}_{lmN}^H}{\omega_{mN}^3} \bar{\mathcal{Z}}_{\omega_{mkn}lmk'n'}^H e^{i\Delta k\Upsilon_\theta\lambda} e^{i\Delta n\Upsilon_r\lambda} + \text{c.c.} \right\rangle. \quad (\text{B40})$$

Next we note that the argument of the exponential is

$$i\lambda(\Delta k\Upsilon_\theta + \Delta n\Upsilon_r) = i\lambda\Upsilon(\Delta k\beta_\theta + \Delta n\beta_r) = i\lambda\Upsilon(N' - N). \quad (\text{B41})$$

Evaluating the average over λ enforces $N = N'$, and the result is

$$\left\langle \frac{dK^\infty}{d\lambda} \right\rangle = \frac{\Gamma}{4\pi} \sum_{lmN} \sum_{(k', n')_N} [\mathcal{M}_{mN} + k'\Upsilon_\theta] \frac{\mathcal{Z}_{lmN}^H}{\omega_{mN}^3} \bar{\mathcal{Z}}_{\omega_{mkn}lmk'n'}^H + \text{c.c.} \quad (\text{B42})$$

Now since $\omega_{mkn} = \omega_{mN} = \omega_{mN'}$, the factor of $\bar{\mathcal{Z}}_{\omega_{mkn}lmk'n'}^H$ can be simplified to $\bar{\mathcal{Z}}_{lmk'n'}^H$. The expression (B42) can then be simplified further by defining the new amplitude

$$\mathcal{Y}_{lmN}^H(\chi_0) = \sum_{(k, n)_N} k \mathcal{Z}_{lmkn}^H(\chi_0) = \sum_{(k, n)_N} k e^{i\xi_{mkn}(\chi_0)} \check{\mathcal{Z}}_{lmkn}^H. \quad (\text{B43})$$

Compare this with Eq. (3.34): $\mathcal{Y}_{lmN}^H(\chi_0)$ is similar to $\mathcal{Z}_{lmN}(\chi_0)$, but with each \mathcal{Z}_{lmkn}^H weighted by k . In terms of this new amplitude the result simplifies to

$$\left\langle \frac{dK^\infty}{d\lambda} \right\rangle = \sum_{lmN} \frac{\Gamma}{4\pi\omega_{mN}^3} [\mathcal{M}_{mN} |\mathcal{Z}_{lmN}^H(\chi_0)|^2 + \Upsilon_\theta \mathcal{Z}_{lmN}^H(\chi_0) \bar{\mathcal{Y}}_{lmN}^H(\chi_0)] + \text{c.c.} \quad (\text{B44})$$

Applying Eqs. (B35) and (B36), we at last find the rate of change of Q for a resonant orbit:

$$\left\langle \frac{dQ^\infty}{dt} \right\rangle = \sum_{lmN} \frac{1}{2\pi\omega_{mN}^3} \{ \mathcal{L}_{mN} |\mathcal{Z}_{lmN}^H(\chi_0)|^2 + \Upsilon_\theta \text{Re} [\mathcal{Z}_{lmN}^H(\chi_0) \bar{\mathcal{Y}}_{lmN}^H(\chi_0)] \}, \quad (\text{B45})$$

where

$$\mathcal{L}_{mN} = m\langle \cot^2 \theta \rangle L_z - a^2 \omega_{mN} \langle \cos^2 \theta \rangle E. \quad (\text{B46})$$

Repeating this exercise for the “down” modes yields

$$\left\langle \frac{dQ^H}{dt} \right\rangle = \sum_{lmN} \frac{\alpha_{lmN}}{2\pi\omega_{mN}^3} \{ \mathcal{L}_{mN} |\mathcal{Z}^\infty(\chi_0)|^2 + \Upsilon_\theta \text{Re} [\mathcal{Z}_{lmN}^\infty(\chi_0) \bar{\mathcal{Y}}_{lmN}^\infty(\chi_0)] \}. \quad (\text{B47})$$

It is interesting to compare our final result for the on-resonance evolution of Q , Eqs. (B45) and (B47), with the equivalent results for the non-resonant case, Eqs. (B37) and (B38). The first two terms in both expressions for $\langle dQ/dt \rangle$ are essentially the same; going from the non-resonant case to the resonant case is simply a matter of promoting the 4-index non-resonant amplitude \mathcal{Z}_{lmkn}^* to the 3-index resonant amplitude \mathcal{Z}_{lmN}^* .

The final term in the two cases is quite different, however. In the non-resonant case, the final term is proportional to $k\Upsilon_\theta$. In the resonant case, the index k cannot appear in the final result, which can only depend on the indices l, m , and N . This is accounted for in the

definition of the amplitude \mathcal{Y}_{lmN}^* , Eq. (B43). In both the non-resonant and the resonant cases, this final term arises from the action of the operator $(d\theta/d\lambda)\partial_\theta$ on the radiative field Ψ_{rad} [see Eq. (B12)].

As Appendix A made clear, the 3-index amplitude \mathcal{Z}_{lmN}^* can be computed directly as a 1-D integral, Eq. (3.45), or can be computed as a sum of 4-index integrals, Eq. (3.34), each of which is computed from the 2-D integral (3.14). Our definition (B43) of \mathcal{Y}_{lmN}^* is clearly analogous to Eq. (3.34), writing this 3-index amplitude as a sum over 4-index amplitudes.

Might it be possible to compute the 3-index amplitude directly, in a manner analogous to Eq. (3.45)? We be-

lieve the answer is yes: We simply need to propagate the operator $(d\theta/d\lambda)\partial_\theta$ under the integral sign in Eq. (3.45). In other words, we speculate that

$$\mathcal{Y}_{lmN}^*(\chi_0) \stackrel{?}{=} \frac{\Upsilon}{\Gamma} \int_0^{2\pi/\Upsilon} d\lambda \frac{d\theta}{d\lambda} \partial_\theta J_{lm\omega}^*[r(\lambda), \theta(\lambda, \chi_0)] e^{iN\Upsilon\lambda}. \quad (\text{B48})$$

We have not yet tested this.

-
- [1] F. Pretorius, Phys. Rev. Lett. **95**, 121101 (2005).
 - [2] M. Campanelli, C. O. Lousto, P. Marronetti, and Y. Zlochower, Phys. Rev. Lett. **96**, 111101 (2006).
 - [3] J. G. Baker, J. Centrella, D.-I. Choi, M. Koppitz, J. van Meter, Phys. Rev. Lett. **96**, 111102 (2006).
 - [4] S. A. Hughes, in *Laser Interferometer Space Antenna — Proceedings of the Sixth International LISA Symposium*, edited by S. M. Merkowitz and J. C. Livas (AIP Conference Proceedings 873, Melville, New York, 2006).
 - [5] C. O. Lousto and Y. Zlochower, Phys. Rev. Lett. **106**, 041101 (2011).
 - [6] U. Sperhake, V. Cardoso, C. D. Ott, E. Schnetter, and H. Witek, arXiv:1105.5391.
 - [7] L. Barack, Class. Quantum Grav. **26**, 213001 (2009).
 - [8] A. Pound, E. Poisson, and B. G. Nickel, Phys. Rev. D **72**, 124001 (2005).
 - [9] E. E. Flanagan and T. Hinderer, Phys. Rev. Lett., submitted; arXiv:1009.4923. Referenced in the text as “FH.”
 - [10] T. Hinderer and E. E. Flanagan, Phys. Rev. D **78**, 064028 (2008).
 - [11] Y. Mino, Phys. Rev. D **67**, 084027 (2003).
 - [12] Y. Mino, Prog. Theor. Phys. **113**, 733 (2005).
 - [13] T. Tanaka, Prog. Theor. Phys. Suppl. **163**, 120 (2006).
 - [14] T. A. Apostolatos, G. Lukes-Gerakopoulos, G. Contopoulos, Phys. Rev. Lett. **103**, 111101 (2010).
 - [15] R. Grossman, J. Levin, and G. Perez-Giz, Phys. Rev. D, submitted; arXiv:1105.5811.
 - [16] R. Grossman, J. Levin, and G. Perez-Giz, Phys. Rev. D, submitted; arXiv:1108.1819.
 - [17] S. Drasco, E. E. Flanagan, and S. A. Hughes, Class. Quantum Grav. **22**, S801 (2005).
 - [18] S. A. Teukolsky, Astrophys. J. **185**, 635 (1973).
 - [19] S. Drasco and S. A. Hughes, Phys. Rev. D **73**, 024027 (2006). Referenced in the text as “DH06.”
 - [20] R. Fujita, W. Hikida, and H. Tagoshi, Prog. Theor. Phys. **121**, 843 (2009).
 - [21] N. Sago, T. Tanaka, W. Hikida, K. Ganz, and H. Nakano, Prog. Theor. Phys. **115**, 873 (2006).
 - [22] C. W. Misner, K. S. Thorne, and J. A. Wheeler, *Gravitation* (Freeman, San Francisco, 1973).
 - [23] W. Schmidt, Class. Quantum Grav. **19**, 2743 (2002).
 - [24] S. Drasco and S. A. Hughes, Phys. Rev. D **69**, 044015 (2004).
 - [25] S. A. Hughes, Phys. Rev. D **61**, 084004 (2000).
 - [26] R. A. Isaacson, Phys. Rev. **166**, 1272 (1968).
 - [27] S. A. Teukolsky and W. H. Press, Astrophys. J. **193**, 443 (1974).
 - [28] S. W. Hawking and J. B. Hartle, Commun. Math. Phys. **27**, 283 (1972).
 - [29] R. Fujita and H. Tagoshi, Prog. Theor. Phys. **112**, 415 (2004).
 - [30] R. Fujita and H. Tagoshi, Prog. Theor. Phys. **113**, 1165 (2005).
 - [31] W. Throwe, S. A. Hughes, and S. Drasco, in preparation. Preliminary version available as W. Throwe, unpublished MIT undergraduate thesis (2010).
 - [32] E. E. Flanagan, T. Hinderer, S. A. Hughes, and U. Ruangsri, in preparation.
 - [33] A. Ori, private communication.
 - [34] D.L. Bosley, J. Kevorkian, Siam J. Appl. Math. **51**, 439 (1991).